— 6 —

Stationary and quasi-stationary eddies in the extratropical troposphere: theory

ISAAC M. HELD

6.1. Introduction

The climatological zonal asymmetries in the atmosphere result from asymmetries in the Earth's surface. The problem of explaining the atmospheric asymmetries is complicated by the fact that some of the relevant surface properties, such as ocean temperature, land-surface albedo and ground wetness, are at least partially conteolled by the atmosphere. Yet, even if one ignores these important feedback processes and simply prescribed boundary conditions, the construction of a theory explaining the atmospheric asymmetries remains a difficult challenge. This is particularly so for the asymmetries within the troposphere, where latent heat release and the mixing of momentum and heat by large-scale transients are both dependent on the boundary conditions and the forced wave structure in ways that are little understood.

There exist several recent reviews of problems associated with stationary eddies on various scales, most notably Smith (1979) and Dickinson (1980) on the effects of orography. The intention in this survey is not to present a systematic review of theory but simply to touch upon some of the theoretical issues that have arisen time and again since the pioneering work of Charney and Eliassen (1949), Bolin (1950) and Smagorinsky (1953) on planetary-scale stationary waves. Among these issues are the following:

1. What is the relative importance of topographic forcing and zonally asymmetric diabatic heating in determining the planetary stationary wave structure?

2. To what extent can the observed low-frequency variability in the atmosphere be associated with anomalous forced waves?

3. Why do barotropic models of topographically forced waves work as well as they do?

4. Are forced stationary waves potentially resonant?

Two additional questions concerning Rossby wave propagation arise naturally in discussions of 3 and 4:

5. Are stationary Rossby waves absorbed or reflected when they encounter low latitude easterlies?

6. In what sense, if any, does the tropopause act as if it were a rigid lid?

Without at least partial answers to basic questions such as these, one is not in a very good position to address the problems mentioned in the opening paragraph, concerning the various and subtle ways in which the stationary eddies interact with latent heat release, large-scale transients and the underlying surface.

We begin by describing the response to orography in three linear models: a barotropic model on a beta-plane channel; a barotropic model on a sphere; and a baroclinic, quasi-geostrophic model on a beta-plane channel. These models illustrate the zonal, meridional and vertical propagation of Rossby waves and raise questions 3–6 in relatively simple settings. The emphasis in these sections is on orographic forcing, not because thermal forcing is unimportant (it is not), but partly because the actual diabatic heating distribution in the troposphere is poorly known, and partly because the problem of thermal forcing is complicated by the dependence of the response on the vertical as well as horizontal structure of the forcing. The linear response to diabatic heating is then briefly discussed in Section 6.5.

Following this review of linear forced wave theory, results from atmospheric general circulation models (GCMs) of relevance for questions 1 and 2 are discussed. A comparison of GCMs with realistic orography and with a flat lower boundary is used to address 1, whereas statistics from a GCM with zonally symmetric lower boundary conditions and, therefore, a zonally symmetric climate are used to attempt to shed some light on 2.

The discussion throughout is restricted somewhat arbitrarily to the problem of explaining the stationary and quasi-stationary eddies in the extratropical Northern Hemisphere troposphere during winter. However, many of the ideas are relevant to the summer season and to the Southern Hemisphere.

6.2 Barotropic model in a beta-plane channel: zonal propagation of Rossby waves

The classic paper by Charney and Eliassen (1949) contains the first attempt at quantitative modelling of planetary-scale stationary waves. Using a baro-tropic model on a beta-plane, linearized about a uniform westerly zonal wind flowing over surface topography, these authors obtained a striking fit to the wintertime 500 mb stationary geopotential field along 45°N. It is worthwhile discussing this calculation in detail both because of its historical importance and because it raises the issue of the potential for resonant behaviour of stationary waves in a very simple context.

Postponing any attempt at justification, consider the equation for con-servation of potential vorticity for the hydrostatic, depth-independent flow of a homogeneous layer of fluid with a free surface:

$$\left(\frac{\partial}{\partial t} + \mathbf{v} \cdot \nabla\right)\left(\frac{f + \zeta}{H}\right) = 0. \tag{6.1}$$

$H = h - h_T$, where H is the layer thickness, h the height of the free surface and h_T the height of the rigid lower boundary. The notation is otherwise conventional. In the quasi-geostrophic approximation on a beta-plane, (6.1) reduces to:

$$\left(\frac{\partial}{\partial t} + \mathbf{v}_g \cdot \nabla\right)q = 0, \tag{6.2}$$

where $q = f_0 + \beta y + \zeta - f_0(\eta - h_T)/h_0$, h_0 is the mean depth, $\eta = h - h_0$, $\mathbf{v}_g = g/f_0 \mathbf{k} \times \nabla \eta$ and $\zeta = (g/f_0)\nabla^2 \eta$ (compare with the general formulation in the Appendix—Eqns. A10 and A11). Linearizing about a zonal flow $[u] = -(g/f_0)\,\partial[\eta]/\partial y$ independent of x, y and t and retaining only the lowest-order term in the topographic forcing, one obtains for the perturbation (denoted by a *)

$$\left(\frac{\partial}{\partial t} + [u]\frac{\partial}{\partial x}\right)q^* + v^*\frac{\partial[q]}{\partial y} = 0, \tag{6.3a}$$

where $q^* = \zeta^* - f_0(\eta^* - h_T)/h_0$ and $\partial[q]/\partial y = \beta + [u]/\lambda^2$ with $\lambda^2 = gh_0/f_0^2$. Substituting for q^* and $\partial[q]/\partial y$ an alternative form of this equation is:

$$\frac{\partial}{\partial t}\left(\zeta^* - \frac{f_0}{h_0}\eta^*\right) + [u]\frac{\partial}{\partial x}\zeta^* + \beta v^* = -[u]\frac{f_0}{h_0}\frac{\partial h_T}{\partial x}. \tag{6.3b}$$

From (6.3a) and (6.3b), the dispersion relation for free plane waves, $\eta^* = \text{Re }\tilde{\eta} \exp i(kx + ly - \omega t)$, is

$$\omega = k\left\{[u] - \frac{\partial[q]}{\partial y}\Big/(k^2 + l^2 + \lambda^{-2})\right\} \tag{6.4a}$$

$$= k\{[u](k^2 + l^2) - \beta\}/(k^2 + l^2 + \lambda^{-2}). \tag{6.4b}$$

(Note that ω is not equal to the frequency of a Rossby wave in the absence of mean flow, Doppler shifted by $k\bar{u}$. As is clear from (6.4a), a 'non-Doppler' effect results from the mean flow being balanced by a height gradient that alters $\partial[q]/\partial y$. As discussed by White (1977), precisely the same effect occurs in a continuously stratified flow, where it enters through the lower boundary condition and has caused some confusion in the literature.) If $[u] < 0$ the system cannot support a stationary Rossby wave, whereas if $[u] > 0$ the total wavenumber of the stationary wave is $k^2 + l^2 \equiv K^2 = \beta/[u] \equiv K_s^2$. This stationary wavenumber is independent of λ. If one is only interested in the stationary flow, and if the flow is quasi-geostrophic, there is no advantage in the use of the divergent rather than non-divergent vorticity equation.

Consider the steady version of Eqn. (6.3) in a channel geometry, assuming that η^* and h_T are both proportional to sin (ly). Fourier analysing in x and denoting Fourier amplitudes by tildes, one finds that:

$$\tilde{\eta} = \tilde{h}_T/[\lambda^2(K^2 - K_s^2)]. \tag{6.5}$$

For $K > K_s$ ($K < K_s$), the response is exactly in (out of) phase with the topography, with the topographic source of vorticity balanced primarily by the zonal (meridional) advection of relative (planetary) vorticity. Following Charney and Eliassen, the resonance singularity is removed by adding Ekman pumping, which amounts to adding a linear damping on the vorticity in this barotropic model. For steady flow, Eqn. (6.3b) is modified to:

$$[u]\frac{\partial\zeta^*}{\partial x} + \beta v^* = -r\zeta^* - \frac{[u]f_0}{h_0}\frac{\partial h_T}{\partial x}, \tag{6.6}$$

resulting in the modified Fourier amplitudes:

$$\tilde{\eta} = \tilde{h}_T/[\lambda^2(K^2 - K_s^2 - i\varepsilon)] \tag{6.7}$$

with $\varepsilon \equiv rK^2/k[u]$.

Charney and Eliassen justify this barotropic model by starting with the quasi-geostrophic vorticity equation and assuming that the flow is separable, $\eta = A(x, y)B(z)$; the choice of vertical structure $B(z)$ is then based on observations. As described in the Appendix, $[u]$ on the lhs of Eqn. (6.6) is re-interpreted as a mid-tropospheric wind, whereas $[u]$ on the rhs is re-interpreted as a surface wind—and then replaced by $0.4[u]$, so that the implied vertical velocities are of reasonable magnitude. A more satisfying procedure for justifying barotropic calculations is discussed in Section 6.4.

The variance of the solution to (6.6), $[\eta^{*2}]$, is plotted in Fig. 6.1 as a function
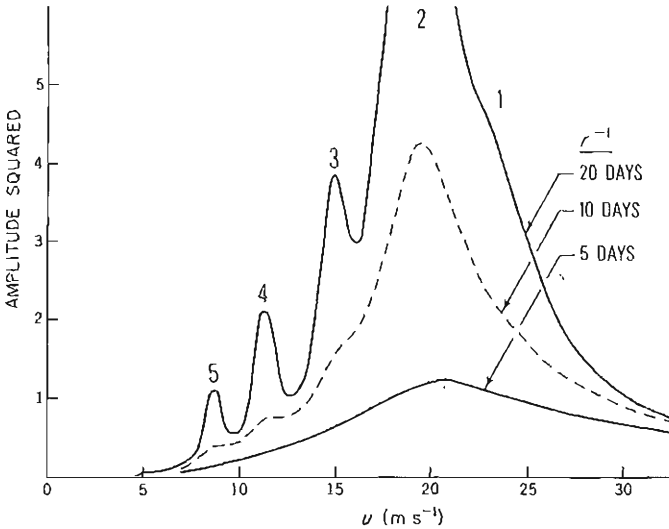
Fig. 6.1. The mean square height response, $[\eta^{*2}]$, in the Charney–Eliassen model as a function of $[u]$ for different strengths of dissipation, in units of 10^4 m^2. The integers mark the values of $[u]$ at which particular zonal wavenumbers resonate.

of $[u]$ for different values of r. The x-dependence of h_T used is obtained from the smoothed topography at 45°N in the GCM discussed in Section 6.6, and is plotted in Fig. 6.2. The meridional wavenumber is chosen so that one half-wavelength equals 35° latitude, while $f_0 = 2\Omega \sin (45°)$ and $h_0 = 8$km. The results show a clear resonance structure when $r^{-1} = 20$ days, with the wavenumber 2 resonance dominant but with 3, 4 and 5 also apparent. Little of this structure remains at $r^{-1} = 5$ days.

Figure 6.2 compares the solution $\eta^*(x)$ for $r^{-1} = 5$ days and $[u] = 17$ m s^{-1} with the climatological 500 mb height at 45° for January. (As in Charney and Eliassen, $[u]$ on the rhs of Eqn. (6.6) has been multiplied by 0.4.) Since thermal forcing contributes a substantial part of this mid-tropospheric eddy field (see Section 6.6), one should consider the excellence of this fit as accidental. It is still of interest, however, that responses of the correct order of magnitude and structure are obtained for values of r sufficiently large that the system does not resonate.

To explore this point further, the total response has been split into two parts in Fig. 6.3, that due to the topography of the Eastern Hemisphere and that due to the topography of the Western Hemisphere. The total response is clearly the sum of two well-defined wavetrains, one emanating from the Rockies and the other, somewhat stronger, from the Tibetan Plateau. Each of the wavetrains decays eastward sufficiently rapidly that there is only modest interference between the two. For this large a dissipation, it is evidently more fruitful to
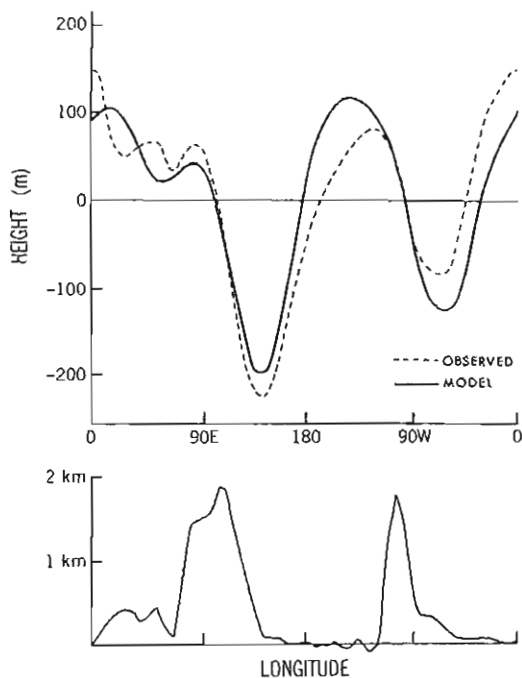
Fig. 6.2. Upper figure: the height response as a function of longitude in the Charney–Eliassen model for the parameters listed in the text (solid line), and the observed climatological 500 mb eddy heights at 45°N in January, from Oort (1982) (dashed line). Lower figure: the topography $h_T(x)$ used in the calculation.
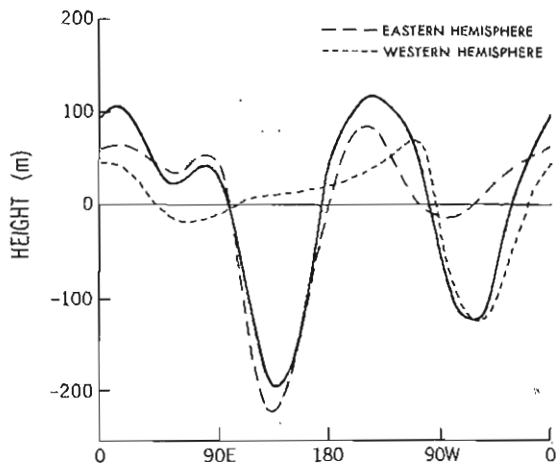
Fig. 6.3. The response shown in Fig. 6.2 split into the parts due to the topography of the western and eastern hemispheres.

think in terms of wavetrains emanating from localized features, that is, Green's functions, rather than Fourier components.

The solution to Eqn. (6.6) on a channel of infinite length can be written, for sufficiently small r, in the form:

$$\eta^*(x, y) = \sin (ly) \int_{-\infty}^{\infty} G(x - x')h_T(x') \, dx', \qquad (6.8)$$

where:

$$G(x - x') = 0 \quad \text{if } x \leqslant x',$$

$$= -\frac{1}{k_s \lambda^2} \sin (k_s(x - x')) \exp \left[-r(x - x')/c_x \right]$$

$$\text{if } x \geqslant x'.$$

$k_s = (K_s^2 - l^2)^{1/2}$ is assumed real, and c_x is the zonal group velocity for non-divergent Rossby waves evaluated at the stationary wavenumber:

$$c_x = \partial\omega/\partial k = 2[u]k_s^2/(k_s^2 + l^2). \qquad (6.9)$$

c_x is always positive and less than $2[u]$. It is because c_x is positive that the response is confined to the east of the source. As long as the width of the mountain is much less than the stationary wavelength, and as long as the wave is damped out before progressing around the latitude circle and returning to the source region, the response will resemble this Green's function. There will be anticyclonic vorticity over the mountain and a trough immediately downstream, with the stationary wavenumber clearly apparent in the response.

In this simple model, the parameter r determines whether or not the picture of the wave field as composed of potentially resonant Fourier components or of damped wavetrains is the most appropriate. The choice $r^{-1} = 5$ days, for which the latter picture seems more appropriate, is rather small for a spin-down time due to surface friction, but there are other potential sources of dissipation in the troposphere, most notably mixing due to large-scale transients. More importantly, waves can also disperse into low latitudes and into the stratosphere, from which they may be unable to return to the region of forcing. We return to this problem in the following sections.

The character of the long-period variability of the forced waves should be markedly different depending on whether or not the waves are potentially resonant. If they are potentially resonant, one expects these low-frequency anomalies to be of global scale. One also expects dramatic variations in amplitude and phase, with $180°$ phase reversals in individual zonal wavenumbers as the flow passes through resonance. In such circumstances, zonal Fourier analysis is clearly illuminating. In contrast, in the non-resonant dissipative or dispersive case one expects anomalies to be local, unless the
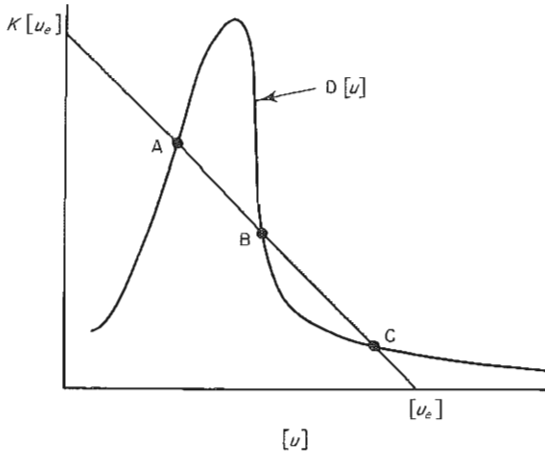
Fig. 6.4. A schematic of the graphic solution for the equilibrium states in the Charney–DeVore model.

mean flow variations happen to be coherent around a latitude circle, and one does not expect Fourier decomposition to provide the simplest picture of the wave field. A simple shift in the wavelength downstream of the Rockies, say, could be disguised as a complex redistribution among several Fourier components.

Resonant behaviour can have more subtle consequences for variability in the atmosphere, as is evident in the intriguing recent work of Charney and Devore (1979) (see also Charney *et al.*, 1981) on the possible importance of wave-mean flow interaction for the maintenance of anomalous forced wave patterns. In the presence of dissipation the steady forced waves generated by topography exert a drag on the zonal flow, $\mathscr{D}([u])$. Following Charney and Devore, suppose that in the absence of this drag the mean flow relaxes to some $[u_e] > 0$, i.e.:

$$\frac{\partial [u]}{\partial t} = -\kappa([u] - [u_e]) - \mathscr{D}([u]). \tag{6.10}$$

$\mathscr{D}([u])$ is the sum of the eddy momentum flux divergence and the form drag, or 'mountain torque',

$$\mathscr{D}([u]) = \frac{\partial}{\partial y}[u^*v^*] + \frac{1}{h_0}[p^* \, \partial h_T/\partial x]$$

$$= -[v^*\zeta^*] - \frac{f_0}{h_0}[v^*h_T]$$

$$= -[v^*q^*]$$

where p^* is the perturbation pressure and q^* is the perturbation potential

vorticity. If the wave consists of only one meridional mode, $\sin(ly)$, one can show that:

$$\mathcal{D}([u]) = \frac{rf_0^2 K^2 |\tilde{h}_T|^2 \sin^2(ly)}{2[u]h_0^2((K^2 - K_s^2)^2 + \varepsilon^2)}. \tag{6.11}$$

Thus, $\mathcal{D}([u])$ has basically the same shape as $[\eta^{*2}]$ in Fig. 6.1.

A graphical solution to the steady-state equation, $\mathcal{D}([u]) = \kappa([u_e] - [u])$ is shown in Fig. 6.4. (For the purposes of this qualitative argument, we ignore the y-variation in $\mathcal{D}([u])$.) If the parameters are such as to produce the graph shown, three possible equilibria exist, labelled A, B and C in the figure. It is intuitively clear from Eqn. (6.10) that if $\kappa + \mathrm{d}\mathcal{D}/\mathrm{d}[u]$ is negative, as it is for B, the state is unstable. The high-index, small-wave amplitude state C is associated by these authors with the 'normal' flow, and the low-index, amplified-wave state A with 'blocking'. Without the resonant structure in $\mathcal{D}([u])$, multiple equilibrium states of this sort do not occur.

6.3 Barotropic model on a sphere: meridional propagation of Rossby waves

6.3.1 Numerical results

These results for barotropic flow in a beta-plane channel are substantially modified when account is taken of the spherical geometry and mean flow variation with latitude, as recently described by Grose and Hoskins (1979). Although these authors study a divergent shallow water model, the free surface has no effect on quasi-geostrophic stationary waves, as described in Section 6.2, and we therefore restrict the following discussion to the spherical version of Eqn. (6.6):

$$\frac{[u]}{a \cos \phi} \frac{\partial \zeta}{\partial \lambda} + v^* \left(\frac{1}{a} \frac{\partial [\zeta]}{\partial \phi} + \beta \right) = \frac{-[u_s]f}{h_0 a \cos \phi} \frac{\partial h_T}{\partial \lambda} - r\zeta^* \tag{6.12}$$

with

$$(u, v) \equiv \left(-\frac{1}{a} \frac{\partial \psi}{\partial \phi}, \frac{1}{a \cos \phi} \frac{\partial \psi}{\partial \lambda} \right).$$

The coefficient r is taken to be independent of latitude.

We describe responses to this equation with h_T equal to the Northern Hemisphere topography used in the GCM described in Section 6.6 and with $h_T = 0$ in the Southern Hemisphere. The topography is shown in Fig. 6.5. $[u]$ and $[u_s]$ are set equal to the zonally averaged 300 mb and surface winds produced by the 'no-mountain' model in Section 6.6, and are shown in Fig. 6.6. The choice of 300 mb winds is guided by the experience of Grose and Hoskins, who
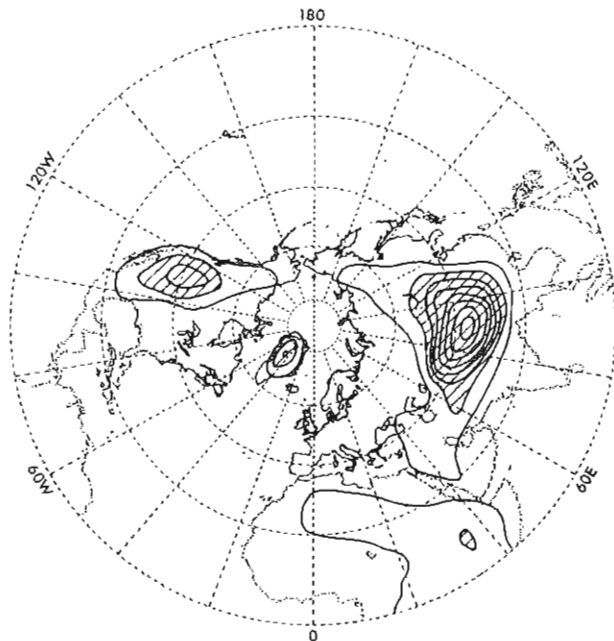
Fig. 6.5. The topography used in the spherical barotropic calculations, taken from the low resolution spectral model described in Section 6.6. The contour interval is 500 m and heights over 1 km are shaded. The zero contour is not shown. The concentric dotted circles are 20° latitude apart, the outer circle being the equator.

find that this choice produces realistic wave patterns. The model's $[u]$ is everywhere positive, so problems associated with 'critical latitudes' (latitudes at which $[u] = 0$) do not arise. The streamfunctions obtained by solving Eqn. (6.12) for two values of r^{-1}, 5 days and 20 days, are shown in Fig. 6.7. The corresponding height fields, computed from the approximation $\eta = f\psi/g$, are shown in Fig. 6.8. Several aspects of these responses are worth noting:

1. The height field response is everywhere less than 60 m. The amplitude at 45°N is more than a factor of three smaller than that obtained with the Charney–Eliassen model, using the identical topography along 45°. Roughly half of this difference in amplitude can be explained by setting h_T in the spherical model equal to $h_T(45°) \sin(ly)$ in the latitude band corresponding to the domain of the Charney–Eliassen model, with $h_T \equiv 0$ outside of this band and with l and $[u_s]$ as in that model. The rest of the difference must be due to the two-dimensional rather than the one-dimensional dispersion of Rossby waves away from localized sources. This particular barotropic model on a sphere, at least, seriously underestimates the amplitude of the orographically forced waves in the mid-troposphere (see Section 6.6).
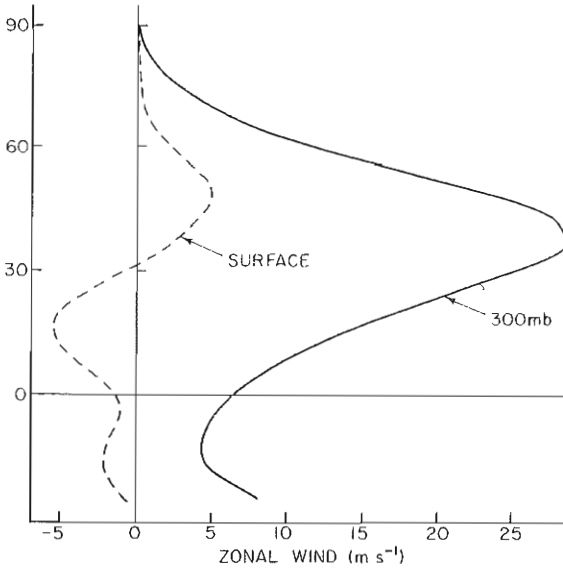
Fig. 6.6. The upper tropospheric and surface winds in the Northern Hemisphere used for $[u]$ and $[u_s]$ in Eqn. (6.12), taken from the 'no-mountain' model described in Section 6.6.
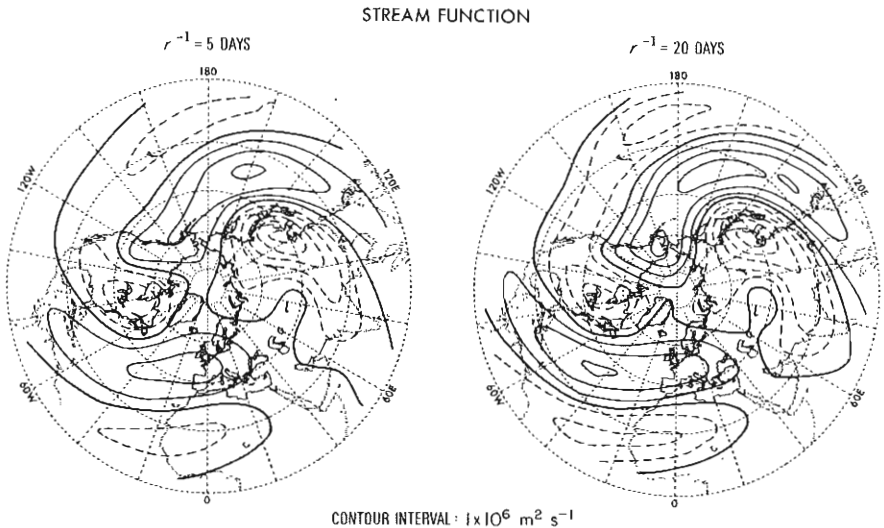
Fig. 6.7. The streamfunction response in the Northern Hemisphere of the barotropic model, using the topography and mean winds in Figs. 6.5 and 6.6, for two different levels of dissipation. Solid contours are positive or zero; dotted contours are negative.

GEOPOTENTIAL

CONTOUR INTERVAL · 10m
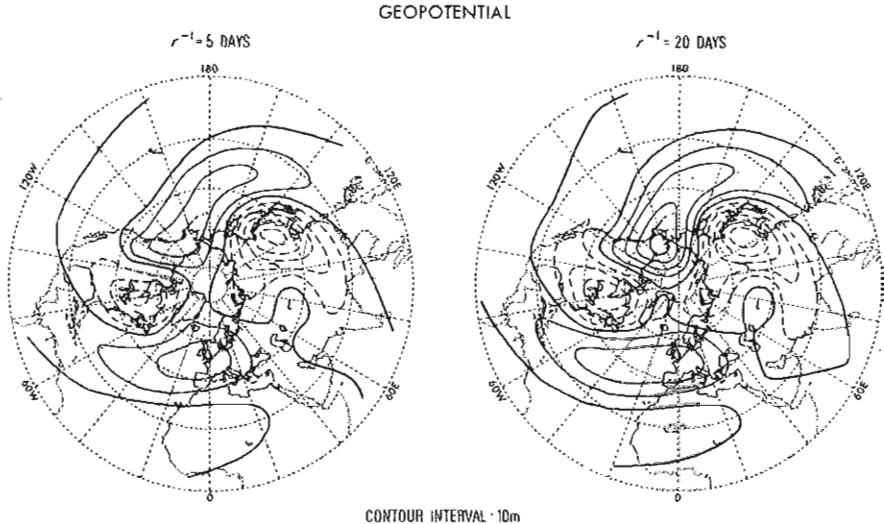
Fig. 6.8. As in Fig. 6.7, but for the height response, $f\psi/g$.

However, comparison with Fig. 2.2 shows the very realistic nature of the pattern obtained.

2. The amplitudes of the dominant troughs downstream of the Tibetan Plateau and the Rockies are nearly identical for the two values of r shown. The perturbations further downstream are naturally more sensitive to the level of dissipation, as is evident in the streamfunction maps in which one can follow the equatorward propagating wavetrains into the tropics. This contrasts sharply with the channel model, in which the amplitude of the entire response is sensitive to the value of r in this range, as is clear from Fig. 6.1.

3. As pointed out by Grose and Hoskins, the geopotential response gives the misleading impression of predominantly zonal propagation because of the factor $f \propto \sin \phi$ multiplying the streamfunction. In contrast, the stream-function responses seem to be dominated by two wavetrains propagating southeastwards, one produced by the Rockies and the other by the Tibetan plateau. Besides these two dominant groups, there are other highs and lows that are with more difficulty associated into wavetrains. The separate responses to the topography of the Eastern and Western Hemispheres are plotted in Fig. 6.9 using $r^{-1} = 20$ days. The interference between these two parts of the response is modest: the Tibetan plateau response decreases the strength of the low in eastern North America by 15%, whereas the response to the Rockies has almost no effect on the low on the east Asian coast. (This result should be sensitive to the structure of the zonal flow, however.) In a.
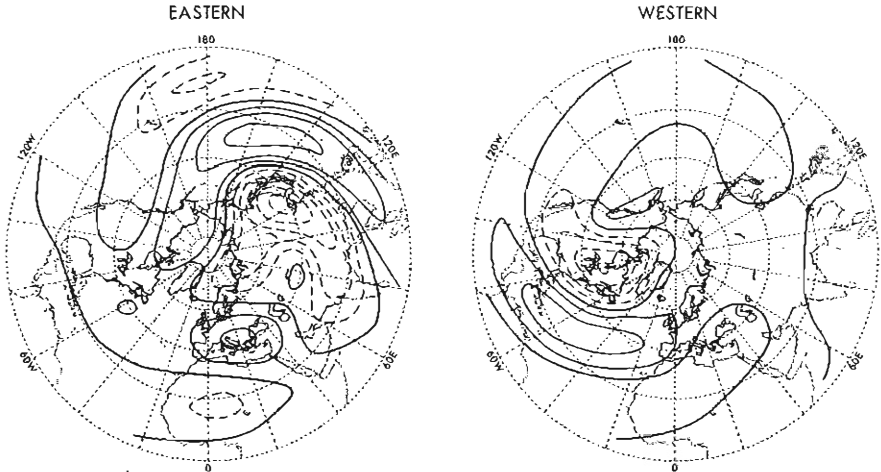
EASTERN

WESTERN

Fig. 6.9. The streamfunction response of Fig. 6.7 with $r^{-1} = 20$ days, split into the responses to the topography of the Eastern and Western Hemispheres.

channel model with the same value of r, interference between the Rocky and Tibetan responses is much more substantial, due to the meridional confinement of the waves.

6.3.2 Meridional dispersion

As noted by Hoskins and Karoly (1981), Rossby wave ray tracing theory explains these structures rather well. For this purpose it is advantageous to transform the linearized unforced inviscid vorticity equation into Mercator coordinates:

$$x = a\lambda; \quad \frac{\mathrm{d}y}{a} = \frac{\mathrm{d}\phi}{\cos\phi},$$

so that:

$$\hat{u}\frac{\partial}{\partial x}\left(\frac{\partial^2}{\partial x^2} + \frac{\partial^2}{\partial y^2}\right)\psi^* = -\hat{\beta}\frac{\partial\psi^*}{\partial x} \tag{6.13}$$

where $\hat{u} \equiv [u]/\cos\phi$ and $\hat{\beta} \equiv \cos\phi(\beta + 1/a\ \partial[\zeta]/\partial\phi)$.

For a wave of the form $\psi' = \mathrm{Re}\ \tilde{\psi}\exp(ikx)$, one has

$$\frac{\partial^2\tilde{\psi}}{\partial y^2} = (k^2 - \hat{\beta}/\hat{u})\tilde{\psi}. \tag{6.14}$$

Given a source localized in latitude, zonal wavenumbers $k > k_s \equiv (\hat{\beta}/\hat{u})^{1/2}$ are meridionally trapped in the vicinity of the source, while wavenumbers $k < k_s$
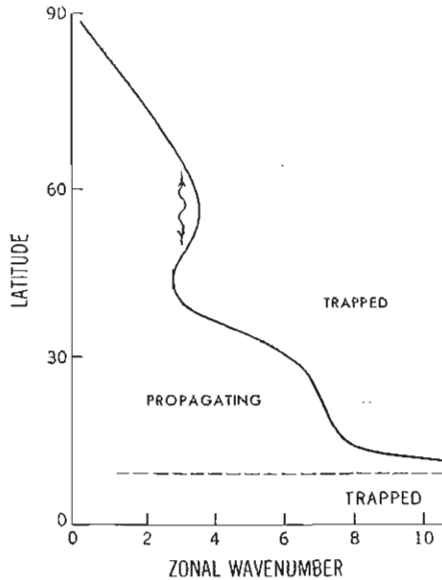
Fig. 6.10. The wavenumber, $n_s = ak_s$, dividing propagating from evanescent solutions for a mean wind resembling the wintertime flow at 300 mb, from Karoly (1978). The arrows indicate the potential for meridional confinement of wavenumber 3 near 55°.

propagate away from the source. Fig. 6.10 taken from Karoly (1978), shows $n_s = ak_s$ as a function of latitude for a particular wintertime 300 mb zonally averaged wind. $n_s \to \infty$ near 10°N, where $[u] = 0$. In the easterlies south of this latitude, all waves are trapped.

A source localized in longitude as well as latitude can be thought of as producing two rays for each $n < n_s$, corresponding to the two possible meridional wavenumbers, $al = \pm(n_s^2 - n^2)^{1/2}$. Since the meridional group velocity of non-divergent Rossby waves, $c_y = \partial\omega/\partial l = 2\hat{\beta}kl(k^2 + l^2)^{-2}$, has the same sign as l, the positive (negative) sign corresponds to poleward (equatorward) propagation. The rays can be traced downstream in the usual way: the zonal wavenumber characterizing the wave group remains unchanged because the mean flow is independent of x, whereas the meridional wavenumber adjusts to satisfy the local dispersion relation; the ray path is tangent to the vector group velocity (c_x, c_y) at this k and l. The amplitude of the streamfunction envelope is proportional to $l^{-1/2}$. One can show further that ray paths are always refracted toward larger 'refractive index' $(n_s^2 - n^2)^{1/2}$, i.e., towards larger n_s, this result being equivalent to Snell's law in optics. At a 'turning latitude', where $n = n_s$, one finds that $l \to 0$, $c_y \to 0$ and an incident poleward propagating wavetrain is simply reflected and continues propagating eastward. At a critical latitude, where $[u] = 0$, $l \to \infty$ but $c_y \to 0$ once again. Rays are refracted into the large region near the critical latitude. In fact,

$c_x/c_y \rightarrow 0$ as $l \rightarrow \infty$, so the rays approaching the critical latitude are oriented north–south. Examples of ray path calculations can be found in Hoskins and Karoly (1981). For zonal flows with uniform angular rotation the rays are great circles. In other cases this is qualitatively true away from critical latitudes, in good agreement with the observations described in Chapter 3.

It is possible for rays to be trapped away from the critical latitude; for example, the ray corresponding to $n = 3$ in Fig. 6.10 is just barely trapped in the high n_s region near 55°. However, waves can be expected to tunnel through the small region of low n_s near 45° and continue propagating into the tropics, so this flow will not provide a very efficient cavity for capturing an $n = 3$ resonance. The form of $n_s(y)$ is sensitive to the curvature of $[u]$, and using climatological wintertime 300 mb winds in Oort (1982), one does not find a well-defined dip in n_s in mid-latitudes. On the other hand, one suspects that substantial changes in curvature occur at particular times, creating more imposing barriers to equatorward propagation, with modest changes in $[u]$ itself. Meridional trapping of this kind is a distinct possibility and may be of importance for the variability of forced waves in the atmosphere. In its absence, however, all rays are eventually attracted into the zero-wind line. The possibility of resonance behaviour then depends on whether or not the complex dynamics in the vicinity of the zero-wind line results in significant reflection of the incident waves.

6.3.3 The critical latitude

If y_c is this critical latitude and if $\partial \hat{u}/\partial y \neq 0$ at $y = y_c$, then $l \propto (y - y_c)^{-1/2}$ and $c_y \propto (y - y_c)^{3/2}$ as $y \rightarrow y_c$. One is tempted to conclude that the packet will never reach y_c, since $\int^y c_y^{-1} \rightarrow \infty$ as $y \rightarrow y_c$. However, this is not the case, since this 'WKB' theory breaks down: WKB predicts that streamfunction amplitude is proportional to $l^{-1/2} \propto (y - y_c)^{1/4}$, so that $(\partial^2 A/\partial y^2)/A \propto (y - y_c)^{-2}$, which eventually grows larger than $l^2 \propto (y - y_c)^{-1}$ as $y \rightarrow y_c$, implying substantial fractional changes in amplitude over one wavelength. With the very small meridional scales generated as y_c is approached, one expects nonlinearity or dissipation of some sort to come into play.

By adding a linear damping $-r\zeta$, to the vorticity equation and then taking the limit of vanishing r, one obtains the familiar result that such a linear dissipative critical layer absorbs incident Rossby waves, at least partially. An indication of this behaviour can be gained without obtaining the explicit solution. Consider the simplest problem of a mean flow with $\hat{u} = u_1 > 0$ for $y > y_1$ and $\hat{u} = u_2 < 0$ for $y < y_2$, where u_1 and u_2 are constants, with a wave incident on the zero-wind line between y_1 and y_2 from the north. From the vorticity equation:

$$\tilde{\zeta} = i\hat{\beta}\tilde{v}/(k\hat{u} - ir),$$

one has:

$$[v^*\zeta^*] = \frac{-\hat{\beta}|\tilde{v}|^2}{2k} Im\left(\frac{1}{\hat{u} - irk^{-1}}\right). \tag{6.15}$$

But:

$$\lim_{\varepsilon \to 0} Im \frac{1}{\hat{u} - i\varepsilon} = \frac{\pi}{|\partial\hat{u}/\partial y|} \delta(y - y_c),$$

where δ is the Dirac delta-function. Since $[v^*\zeta^*] = -(\partial/\partial y)[u^*v^*]$, $[u^*v^*]$ must be constant with latitude in the limit $r \to 0$, except for a jump at the critical latitude:

$$[u^*v^*]|_{y > y_c} = [u^*v^*]|_{y < y_c} + \frac{\pi\hat{\beta}|\tilde{v}|^2}{2k|\partial\hat{u}/\partial y|}\bigg|_{y=y_c} \tag{6.16}$$

In the constant $\hat{u}$ easterly region, $\tilde{\psi} \propto \exp(l_2 y)$, so that $[u^*v^*] = 0$, whereas in the constant $\hat{u}$ westerly region the solution has the form of an incident wave (with amplitude normalized to unity) plus a reflected wave, $\tilde{\psi} \propto \exp(-il_1 y) + R \exp(il_1 y)$, so that

$$[u^*v^*]|_{y > y_c} = \frac{kl_1}{2}(1 - |R|^2) = \frac{\pi\hat{\beta}|\tilde{v}|^2}{2k|\partial\hat{u}/\partial y|}\bigg|_{y=y_c}. \tag{6.17}$$

Assuming that $\hat{\beta} > 0$ and $|\tilde{v}|^2 \neq 0$ at y_c, we must have $|R|^2 < 1$. Part of the incident wave has been absorbed, decelerating the mean flow in the process. The amount of absorption is dependent on $|\tilde{v}|^2$, and its determination generally requires an explicit solution. Dickinson (1968) shows that the absorption is complete if the region in which WKB is valid overlaps with the region around the critical latitude within which $\hat{\beta}/\hat{u}$ can be replaced by $\gamma(y - y_c)^{-1}$, with γ a constant.

The physical relevance of this absorbing critical layer has been questioned in light of the work of Benney and Bergeron (1969) on the possibility of a nonlinear balance in the critical layer. For a discussion of this theory in an atmospheric context, see Tung (1979). Benney and Bergeron's solution matches asymptotically to a linear solution far from the critical layer, consisting of incident and reflected waves of equal magnitudes. Simplified wave-mean flow calculations (Geisler and Dickinson, 1974) suggest one way of understanding these reflections: the waves modify the mean flow in the vicinity of y_c in such as way as to drive $\hat{\beta}$ close to zero; Eqn. (6.17) then implies that $|R| = 1$. The realizability of a strongly reflecting critical layer remains a problem of fundamental importance for stationary wave theory.

If the equatorward propagating waves are organized into localized wavetrains, several additional problems arise concerning the critical latitude. The nonlinear critical layer solution matches onto incident plus reflected waves of a single zonal wavenumber. It is not clear that the behaviour of an

Fig. 6.11. Schematic of the Rossby wavetrain generated by the Tibetan plateau propagating into the tropics.

incident packet localized in longitude can be inferred from this solution or if nonlinearity results in significant coupling of different zonal wavenumbers. Also, the two dominant wavetrains in Fig. 6.9 enter the tropics in the central Pacific and in the Atlantic and should, therefore, be more sensitive to the structure of the zonal wind in these regions than to the zonal mean of the zonal wind. The areas of easterly zonal flow at 200 mb in the time mean January flow taken from Newell *et al.* (1974) are indicated by the shaded areas in Fig. 6.11. The regions of westerlies in the equatorial western Pacific and the Atlantic suggest the possibility that these wavetrains partially avoid zero-wind lines. This idea is returned to in Section 9.5.1.

Some of the low-frequency variability in the extratropical height field is known from the work of Horel and Wallace (1981) and others to be correlated with equatorial Pacific sea-surface temperatures and the phase of the southern oscillation (Fig. 3.10). The direct forcing by a tropical thermal source of a poleward propagating Rossby wave seems to be the simplest explanation for this teleconnection, as suggested by Hoskins and Karoly (1981). But the southern oscillation also involves large changes in the upper tropospheric zonal winds over the Pacific. If one accepts the idea of significant reflection from the easterlies, one can conceive of the amount of reflection of the incident wavetrain as being dependent on the phase of the southern oscillation—an alternative way of generating variability in the poleward propagating waves over North America, as illustrated schematically in Fig. 6.11.

The solutions described by Figs. 6.7–6.9 are obtained for a flow with $\bar{u} > 0$ everywhere, so the waves simply propagate into the Southern Hemisphere. The values of r chosen are sufficiently large that the waves do not return to the Northern Hemisphere with significant amplitude. Thus, these solutions

Fig. 6.12. The height response with $r^{-1} = 20$ days in a calculation identical to that in Fig. 6.8, except for the placement of a perfectly reflecting wall at the equator.

should be very similar to those obtained for a mean flow with an absorbing zero-wind line in low latitudes. In order to examine the implications of significant reflections, we modify these calculations by placing a perfectly reflecting wall at the equator. [As Tung (1979) points out, a reflecting wall does not produce the correct phase of the reflected wave, so this should not be viewed as an attempt at computing the detailed effects of a nonlinear critical layer.] With $r^{-1} = 5$ days, this modification produces little change in the midlatitude response, there being insufficient time for propagation to the tropics and back. The height response for $r^{-1} = 20$ days is shown in Fig. 6.12, to be compared with Fig. 6.8. With this small dissipation, considerable modification of amplitude and phase results in midlatitudes, along with a reduction in the southwest–northeast tilt of the highs and lows. If one repeats these calculations with $[u]$ multiplied everywhere by a constant μ, one finds very little sensitivity to these mean flow changes in the absence of reflections, but with a reflecting wall one finds a modest resonant-like response at $\mu \approx 1.1$, in particular. Not surprisingly, the introduction of the reflecting wall reintroduces the sensitivity to mean winds and to the level of dissipation seen in the beta-channel model, although not in as extreme a form.

Is there evidence in observations for the reflection of Rossby waves? One clue is the observed correlation coefficient between the stationary eddy u^* and

v^* at the maximum in poleward momentum flux near the tropopause at 30°N. Pure equatorward propagation in an inviscid atmosphere in the WKB approximation produces a correlation of $+1$, whereas perfect reflection from the tropics results in standing oscillations with $[u^*v^*] = 0$. The observed correlation is ≈ 0.4 in Oort and Rasmusson (1971), which implies predominantly equatorward propagation but with significant admixture of a poleward component. [This value for the correlation coefficient could be a significant underestimate, however; Mak (1978) finds a much larger $[u^*v^*]$ than do Oort and Rasmussen, for instance.] The linear calculations without a reflecting wall, Figs. 6.7–6.9, yield correlations at 30° close to 0.9. In the calculations with a reflecting wall, the correlation coefficient decreases from ≈ 0.9 at $r^{-1} = 5$ days to ≈ 0.5 at $r^{-1} = 20$ days. It seems that reflection sufficient to produce a correlation similar to that observed is also sufficient to produce weak resonant-like behaviour. However, an alternative explanation for the observed low correlation exists: the poleward propagating component could simply be thermally forced from the tropics (see Section 9.5.2). Indeed, Simmons (1982) has recently argued that tropical diabatic heating may force a significant part of the extratropical stationary eddy field.

6.4 Baroclinic model in a beta-plane channel: vertical propagation of Rossby waves

Just as meridional dispersion of Rossby waves is capable of fundamentally altering the response to topography, so is vertical dispersion. A quasi-geostrophic model on a beta-plane channel, linearized about a mean flow dependent only on height, is the simplest framework in which one can discuss vertical propagation and structure. The concept of vertically propagating Rossby waves was introduced by Charney and Drazin (1961). The use of a baroclinic quasi-geostrophic model for the stationary wave problem was initiated by Smagorinsky (1953) in his study of the response to thermal forcing.

In the absence of diabatic heating, the quasi-geostrophic thermodynamic equation with $z \equiv H \ln (p_*/p)$ as vertical coordinate,

$$\frac{\partial}{\partial t}\left(\frac{\partial \psi}{\partial z}\right) + J\left(\psi, \frac{\partial \psi}{\partial z}\right) = -\frac{N^2}{f_0} W \tag{6.18}$$

when combined with the vorticity equation,

$$\frac{\partial}{\partial t} \nabla^2 \psi + J(\psi, \nabla^2 \psi + \beta y) = \frac{f_0}{\rho_0}\frac{\partial}{\partial z} (\rho_0 W), \tag{6.19}$$

yields the pseudo-potential vorticity equation:

$$\frac{\partial q}{\partial t} + J(\psi, q) = 0,$$

where

$$q \equiv \nabla^2 \psi + \beta y + \frac{f_0^2}{\rho_0} \frac{\partial}{\partial z} \left(\frac{\rho_0}{N^2} \frac{\partial \psi}{\partial z} \right),$$

$$W \equiv \mathrm{d}z/\mathrm{d}t,$$

and

$$\rho_0 \equiv \exp(-z/H).$$

The lower boundary condition is obtained from Eqn. (6.18), after recognizing the relation between W and the actual vertical velocity w,

$$w = \frac{f_0}{g} \frac{\partial \psi}{\partial t} + \frac{RT}{gH} W.$$

Choosing $H = RT(0)/g$, then

$$W = -\frac{f_0}{g} \frac{\partial \psi}{\partial t} + \mathbf{v} \cdot \nabla h_T + \alpha \zeta \qquad (6.20)$$

at the ground, in the presence of topography and Ekman pumping represented by the last term. Linearizing about a mean wind $[u]$ dependent only on z, and once again retaining only the lowest order term in the topographic forcing, one finds:

$$\frac{\partial q^*}{\partial t} + [u] \frac{\partial q^*}{\partial x} + v^* \frac{\partial [q]}{\partial y} = 0 \qquad (6.21)$$

with the boundary condition:

$$\frac{\partial}{\partial t} \left(\frac{\partial \psi^*}{\partial z} - \frac{N^2}{g} \psi^* \right) + [u] \frac{\partial}{\partial x} \frac{\partial \psi^*}{\partial z} - v^* \frac{\partial [u]}{\partial z}$$

$$= -\frac{N^2}{f_0} \left([u] \frac{\partial h_T}{\partial x} + \alpha \nabla^2 \psi^* \right) \quad \text{at } z = 0, \qquad (6.22)$$

where:

$$\frac{\partial [q]}{\partial y} \equiv \beta - \frac{f_0^2}{\rho_0} \frac{\partial}{\partial z} \left(\frac{\rho_0}{N^2} \frac{\partial [u]}{\partial z} \right).$$

Stationary solutions to Eqn. (6.21)–(6.22) exist of the form:

$$\psi^* = \sin(ly) \, \mathrm{Re} \left[\tilde{\psi}(z) \exp(ikx) \right]$$

provided that:

$$\frac{f_0^2}{\rho_0} \frac{\partial}{\partial z} \left(\frac{\rho_0}{N^2} \frac{\partial \tilde{\psi}}{\partial z} \right) = \tilde{\psi} \left(K^2 - \frac{\partial [q]/\partial y}{[u]} \right) \qquad (6.23)$$

and

$$[u]\frac{\partial\tilde{\psi}}{\partial z} - \frac{\partial[u]}{\partial z}\tilde{\psi} = -\frac{N^2[u]}{f_0}\tilde{h}_T - \frac{i\alpha N^2 K^2}{kf_0} \quad \text{at } z = 0.$$

In addition, a radiation condition must be satisfied at infinity.

In the simplest case of constant $[u]$ and N^2, and with $\alpha = 0$, the change of variables $\tilde{\xi} \equiv \tilde{\psi}\exp(-z/2H)$ yields:

$$\frac{\partial^2\tilde{\xi}}{\partial z^2} = \tilde{\xi}\frac{N^2}{f_0^2}(K^2 + \gamma^2 - \beta/[u]) \quad \text{.} \tag{6.24a}$$

and

$$\frac{\partial\tilde{\xi}}{\partial z} + \frac{1}{2H}\tilde{\xi} = -\frac{N^2}{f_0}\tilde{h}_T \quad \text{at } z = 0, \tag{6.24b}$$

where $\gamma \equiv f_0/(2NH)$. If $K^2 + \gamma^2 - \beta/[u] < 0$, that is, if $0 < [u] < \beta/(K^2 + \gamma^2)$, the interior equation has the solutions $\tilde{\xi} = \tilde{\xi}_0\exp(imz)$ with:

$$m = \pm\frac{N}{f_0}\left(\frac{\beta}{[u]} - K^2 - \gamma^2\right)^{1/2}. \tag{6.25}$$

From the time-dependent problem [Eqn. (6.21)] one finds the dispersion relation for vertically propagating waves:

$$\omega = [u]k - \frac{\beta k}{K^2 + \dfrac{m^2 f^2}{N^2} + \gamma^2}, \tag{6.26}$$

from which it follows that the vertical group velocity $(\partial\omega/\partial m)$ has the same sign as m. Therefore, the plus sign in Eqn. (6.25) corresponds to a wave propagating upwards from the source at the ground and is the acceptable solution. If $K^2 + \gamma^2 - \beta/[u] > 0$, that is, if either $[u] < 0$ or $[u] > \beta/(K^2 + \gamma^2)$, then the solution is $\tilde{\xi} = \tilde{\xi}_0\exp(-\mu z)$ with:

$$\mu \equiv \frac{N}{f_0}(K^2 + \gamma^2 - \beta/[u])^{1/2}. \tag{6.27}$$

Employing the boundary condition [Eqn. (6.24b)] one finds:

$$\tilde{\xi}_0 = -\frac{N^2 h_T}{f_0}\left[\binom{im}{-\mu} + \frac{1}{2H}\right]^{-1} \tag{6.28}$$

for the $\binom{\text{propagating}}{\text{trapped}}$ case.

From Eqn. (6.28) one sees that a resonance occurs if $\mu = (2H)^{-1}$, corresponding to $K^2 = K_s^2 \equiv \beta/[u]$. This external Rossby wave is a solution of the unforced inviscid equations with $\tilde{\psi} \equiv 1$ and therefore has no vertical

$[v]$ = const

AMPLITUDE

PHASE

180°

90°

0

←—PROPAGATING—→|←——TRAPPED——→
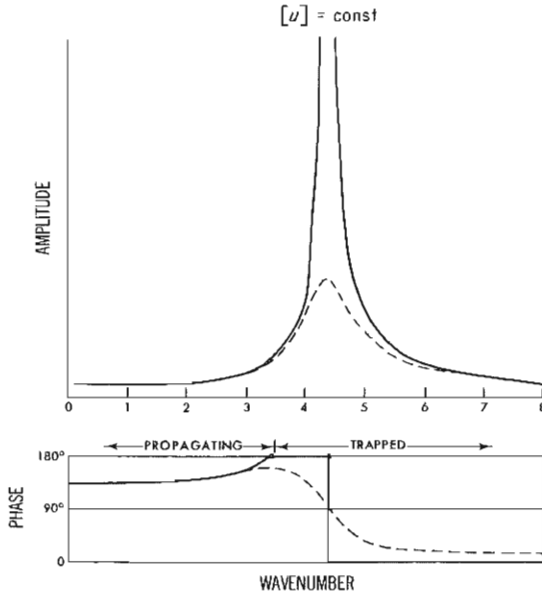
WAVENUMBER

Fig. 6.13. Amplitude and phase of the geopotential height response at $z = 0$ for constant mean wind, as a function of zonal wavenumber. Solid line is for inviscid flow and dotted line for $H/(f_0 \alpha) = 5$ days. A phase of $0°$ implies a response in phase with the topography. A phase between $0°$ and $180°$ implies the ridge in the response upstream from the ridge in the topography.

variation in amplitude or phase. For $K > K_s$, the forced wave solutions decay away from the surface with no phase variation with z, and are exactly in phase with the topography. For $(K_s^2 - \gamma^2)^{1/2} < K < K_s$, $\tilde{\psi}$ increases with height, although not so fast as to prevent $\rho_0|\tilde{\psi}|^2$ from decreasing with height. The solution is equivalent barotropic once again but is now $180°$ out of phase with the topography. For $K < (K_s^2 - \gamma^2)^{1/2}$, $\rho_0|\tilde{\psi}|^2$ is independent of z, the phase shifts westward with height and $\overline{[v^* \, \partial\psi^*/\partial z]} > 0$, and the surface response lags the topography by an amount between $90°$ and $180°$, depending on wavenumber.

Figure 6.13 shows the amplitude and phase of the height response at the ground as a function of total wavenumber for $\alpha = 0$ and for $r^{-1} = H/(\alpha f_0) = 5$ days. The other parameter values are $f_0 = 2\Omega \sin(45°)$, $H = R(275K)/g$, $[u] = 15$ m s^{-1}, $N^2 = 1.0 \times 10^{-4}$ s^{-2}, h_T = constant independent of k, and $l = 0$. The structure is similar to that obtained in the barotropic channel model in that there is one and only one resonance for a given mean flow and meridional modal structure, with the response shifting in phase by $180°$ as the system passes through resonance. The important difference, of course, is the transition to upward propagating waves at small K. (It is because of the choice of zero meridional wavenumber that an equivalent barotropic spin down time
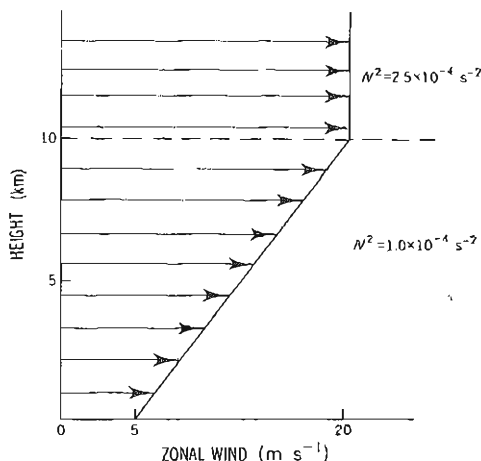
Fig. 6.14. Zonal wind profile and static stabilities used for calculations described in Figs. 6.15–6.18.

of 5 days has less of an effect in Fig. 6.13 than in the barotropic channel model. For non-zero l, the effective strength of the damping is increased by the factor $(k^2 + l^2)^{1/2}/k$.)

Consider now the more realistic model atmosphere shown in Fig. 6.14, with $[u]$ increasing linearly from 5 m s^{-1} at $z = 0$ to 20 m s^{-1} at $z = 10$ km, and with $N^2 = 1.0 \times 10^{-4}$ and 2.5×10^{-4} s^{-2} for $z < 10$ km and $z > 10$ km, respectively. The critical wavenumber:

$$K_c(z) \equiv \left(\frac{\partial[q]/\partial y}{[u]} - \frac{f_0^2}{4N^2H^2} \right)^{1/2} \tag{6.29}$$

dividing the locally wavelike from the locally evanescent solutions is plotted in Fig. 6.15. (All other parameters are identical to those used in the constant wind case.) Note that $\partial[q]/\partial y = \beta$ for $z > 10$ km, while $\partial[q]/\partial y = \beta(1 + h/H)$ in the troposphere, where $h \equiv f_0^2 (\partial[u]/\partial z)/(\beta N^2)$. h/H is of order unity, so there is a substantial discontinuity in $\partial[q]/\partial y$ and, therefore, in K_c at the tropopause. (The discontinuity in $f_0^2/(4N^2H^2)$ in Eqn. (6.29) is of less consequence.) For $K < K_1 \simeq 3.7$, the forced wave propagates on both sides of the tropopause, for $K_1 < K < K_2 \simeq 5.9$, the wave has a turning point precisely at the tropopause, while for $K > K_2$, the wave has a turning point within the troposphere.

All of the waves that are evanescent above some height Z_T (that is, all $K > K_1$) are equivalent barotropic. The proof follows from the fact that $[v^*q^*] = 0$ (easily obtained from the equation of motion, $[u] \partial q^*/\partial x + v^* \partial[q]/\partial y = 0$) and the kinematic identity:

$$[v^*q^*] = -\frac{\partial}{\partial y}[u^*v^*] + \frac{f_0^2}{\rho_0}\frac{\partial}{\partial z}\left(\frac{\rho_0}{N^2}[v^* \, \partial\psi^*/\partial z] \right). \tag{6.30}$$
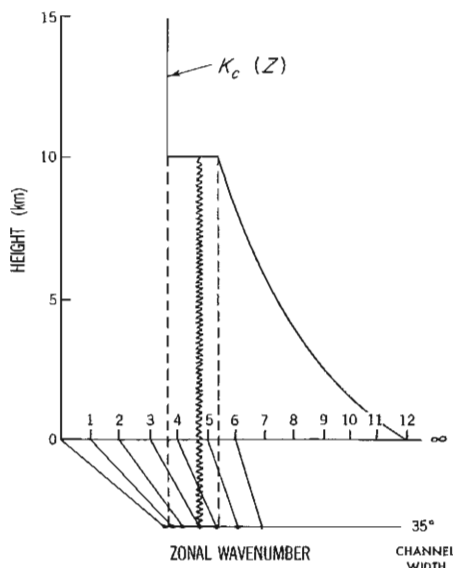
Fig. 6.15. The critical total wavenumber, $K_c(z)$, dividing the locally propagating ($K < K_c$) from the locally evanescent solutions ($K > K_c$). The zonal wavenumber which yields this total wavenumber if the meridional structure is a half wavelength sine wave in a channel of width 35° is also indicated. The wavy line marks the wavenumber of the stationary external Rossby wave.

$[u^*v^*] = 0$ for   waves   of   the   form $\sin(ly) \operatorname{Re} \{\tilde{\psi} \exp(ikx)\}$,   so $\rho_0 N^{-2}[v^* \partial\psi^*/\partial z]$ must be independent of height. There is no heat flux at infinity if the waves are evanescent above Z_T; therefore, the heat flux and the related vertical phase variation must be identically zero at all heights, except for possible 180° phase shifts. In effect, these trapped waves are composed of upward and downward propagating components of equal magnitude.

Figure 6.16 shows the amplitude and phase of the height response at the ground for this profile. There is considerable similarity with the analogous plot for $[u] = \text{constant}$. There is once again a single resonance, corresponding to a stationary external Rossby wave, located at $K = K_R = 4.7$ for the parameters chosen. The resonance happens to lie within the range $K_1 < K < K_2$ for which the waves have a turning point precisely at the tropopause. Figure 6.17 is a plot of the Rossby wave's vertical structure. The maximum at the tropopause can be understood from the WKB wavefunction noted in the figure: $\tilde{\psi}$ increases with increasing z within the troposphere partly because of the $\exp(z/2H)$ factor and partly because $m = Nf_0^{-1}(K_c^2 - K^2)$ decreases with height; the decay above the tropopause results from μ being larger than $(2H)^{-1}$. If $\partial[u]/\partial z$ were negative rather than zero in the model stratosphere, this decay would be more rapid.
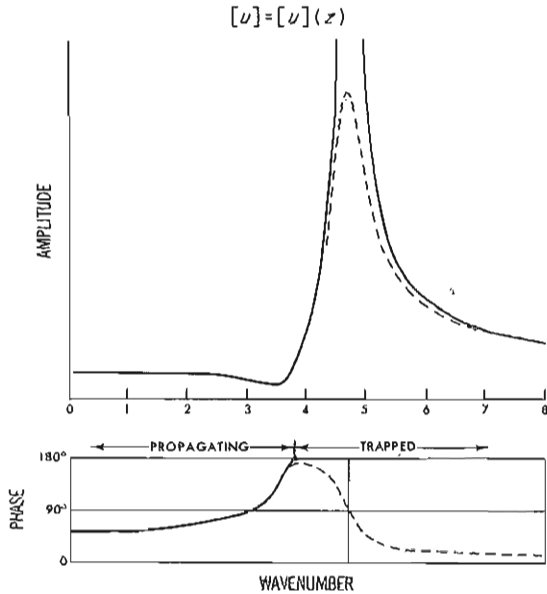
Fig. 6.16. Same as Fig. 6.13 for the wind profile shown in Fig. 6.14.
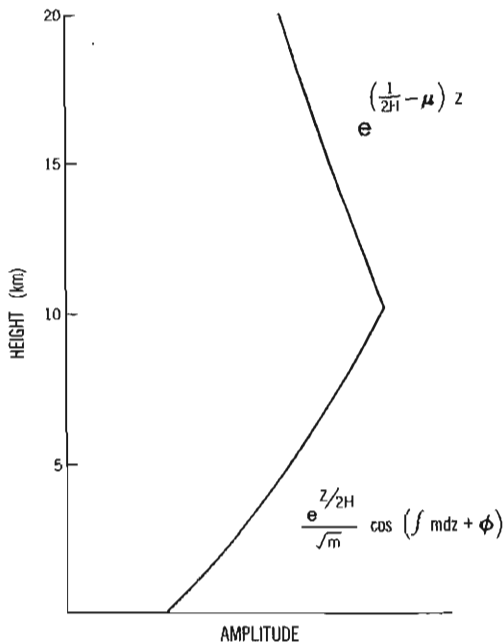
Fig. 6.17. The vertical structure of the external Rossby wave as computed numerically. The expressions alongside the curve are the WKB approximations to this structure.

The importance of the span of wavenumbers $K_1 < K < K_2$ for which the tropopause acts like a perfect reflector in this model atmosphere is enhanced by the fact that it contains the external Rossby wave. Furthermore, for a given meridional scale, $l \neq 0$, this range of total wavenumbers translates into a larger range of zonal wavenumbers. In Fig. 6.15, the lower horizontal axis is labelled with the appropriate zonal wavenumbers for the fundamental meridional mode in a channel of width 35°. For this mode, close to that used by Charney and Eliassen, zonal wavenumbers 1 through 4 all have turning points at the tropopause.

If one defines z_R such that $(\beta/[u(z_R)])^{1/2} = K_R$, then $z_R \simeq 6.7$ km ($p_R \sim 430$ mb) for these parameters. Repeating these calculations for various values of the tropospheric shear (holding all other parameters fixed, including the surface wind), one finds that larger shears result in larger z_R, but the changes are modest. z_R increases from $\simeq 6.2$ km at a shear of 1×10^{-3} s^{-1} to $\simeq 7.2$ km at 3×10^{-3} s^{-1}. Holding the shear fixed at 1.5×10^{-3} and varying $[u(0)]$, z_R varies monotonically from $\simeq 6.85$ km at $[u(0)] = 2.5$ m s^{-1} to 6.4 km at $[u(0)] = 10$ m s^{-1}. The application of Rossby's stationary wave formula in all cases requires the choice of an upper tropospheric wind in order to produce the correct wavelength of the stationary external wave.

Just as in the barotropic model, at times the response may be more easily understood in terms of Green's functions rather than Fourier components. The Green's functions for Eqns. (6.21)–(6.22) [more precisely, the solution when $h_T = \sin(ly) \, \delta(x)$] is shown in Fig. 6.18. l is chosen to correspond to the fundamental mode in a channel of width 42.5°, so that zonal wavenumbers 1 and 2 propagate into the stratosphere whereas 3 does not, and $H/(\alpha f_0)$ is set equal to 5 days. (This solution is obtained by Fourier analysing in x and retaining only the first 15 zonal harmonics, so the structure in the immediate vicinity of the source is somewhat distorted.) Within the troposphere one sees an equivalent barotropic wavetrain propagating eastward from the source with maximum amplitude near the tropopause, of wavelength close to that of the external mode. If one modifies l, the zonal wavelength of this tropospheric response changes so as to maintain constant K. Amplitudes increasing with height in the stratosphere are primarily confined to longitudes slightly east of the source. If one thinks of the source in Fig. 6.18 as the Tibetan plateau, then the dominant high in the stratosphere can be associated with the Aleutian anticyclone.

Some insight into the structure of this Green's function can be gained by using ray tracing theory in the zonal-vertical plane. The ratio of vertical to zonal group velocities $(\partial \omega/\partial m)/(\partial \omega/\partial k)$ is $(m/k)(f/N)^2$, where m is obtained from the local dispersion relation for stationary waves. Evaluating this ratio, one finds that the waves propagate through the troposphere while moving only 10°–30° longitude downstream, consistent with Fig. 6.18. A similar calculation can be found in Hayashi (1981), where one also finds a discussion of why this
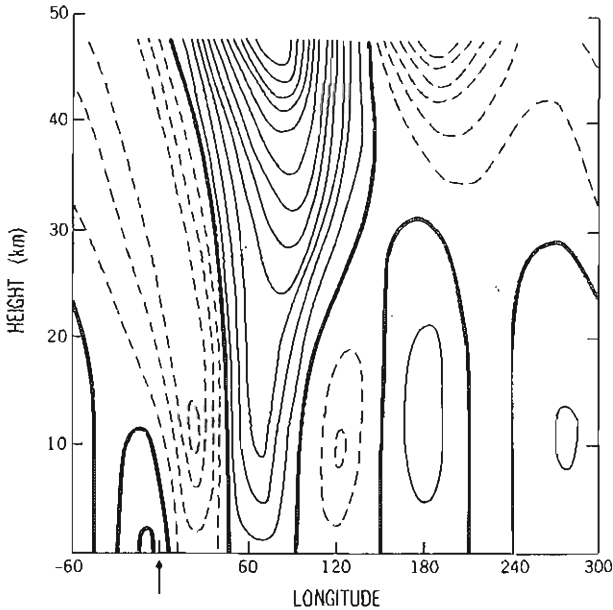
Fig. 6.18. The solution to Eqns. (6.21)–(6.22) with $h_T(x) = \delta(x)\,\sin(ly)$. The arrow marks the location of the source. Solid lines are positive contours and dotted lines negative.

group velocity argument works even though the 'group' consists only of wavenumbers 1 and 2. Because of this rapid vertical propagation, a short distance downstream from the source one is left with only those waves reflected from turning points at or below the tropopause. But of these, all are destroyed as they travel downstream by destructive interference between the upward and downward propagating components, except for the external Rossby wave, which then dominates the far field. This picture is confirmed by standard asymptotic analysis.

If $[u]$ is allowed to increase with height indefinitely, or if it is given a realistic structure with a mesospheric as well as tropospheric jet, then there can exist additional stationary normal modes (e.g., Geisler and Dickinson, 1975; Tung and Lindzen, 1979). These internal modes are still equivalent barotropic but differ from the external, or fundamental, vertical mode in having more structure in the vertical, with maximum amplitudes at turning points in the middle atmosphere. If significant reflections from upper level winds occur, whether or not the system is capable of exciting the vertical normal modes created by these reflections, stratospheric and mesospheric winds will have some impact on the tropospheric forced wave structure. Unless a particular internal mode is selectively amplified, however, it seems unlikely that waves

reflected from the middle atmosphere can dominate over the more easily excited external Rossby waves.

The analysis of forced wave responses in numerical general circulation models is further complicated by the possibility of artificial internal modes created by reflection from the model's upper boundary. For example, in a two-layer model without vertical shear in $[u]$, the two vertical modes have phase speeds $[u] - \beta/(k^2 + l^2)$ and $[u] - \beta/(k^2 + l^2 + \lambda^{-2})$, where λ is here the internal radius of deformation. Comparison with the results for a semi-infinite atmosphere with constant $[u]$ shows that the second of these modes is artificial. Fortunately, this mode has minimum eastward phase speed $[u] - \beta\lambda^2$, so it can only be stationary if $[u] < \beta\lambda^2$. In the presence of vertical shear, one can demonstrate that only one of the two modes can be stationary if the *vertically averaged* zonal mean flow is larger than $\beta\lambda^2$. This condition is typically met in mid-latitudes: $\frac{1}{2}([u]_1 - [u]_2) > \beta\lambda^2$ is the condition for baroclinic instability, where subscripts 1 and 2 refer to the upper and lower layers, respectively. Therefore, an unstable or marginally stable state with $[u]_2 > 0$ also has $\frac{1}{2}([u]_1 + [u]_2) > \beta\lambda^2$. It is generally the case in multi-level models as well that the artificial internal modes have intrinsic phase speeds that are too small for them to be stationary in a midlatitude wintertime flow. Some distortion of the tropospheric stationary waves resulting from the artificial upper boundary condition imposed in GCM's is undoubtedly present, particularly in the longest waves, but it has yet to be evaluated in a realistic three-dimensional context.

As is clear from Fig. 6.5, topographic sources on the Earth are quite localized. If the external Rossby wave does indeed dominate the far field, as in the simple model atmosphere of Fig. 6.14, then the response in most regions should have the horizontal and vertical structure of this external mode. This picture suggests that ray tracing in the horizontal should be performed using the local dispersion relation of the stationary external Rossby wave as determined by the quasi-geostrophic model with local values of $[u]$, $\partial[q]/\partial y$, and N^2, thus eliminating any ambiguity in the choice of equivalent barotropic level, Z_R. In fact, Z_R will then be a slowly varying function of position. It is the rapid adjustment to this particular modal structure in the vertical, much more rapid than the adjustment in the horizontal, which is responsible for the relevance of barotropic calculations and two-dimensional ray tracing theory.

6.5 Thermal forcing

In the presence of diabatic heating, the quasi-geostrophic thermodynamic equation for linear, stationary eddies is modified to read:

$$[u]\frac{\partial}{\partial x}\frac{\partial \psi^*}{\partial z} - \frac{\partial \psi^*}{\partial x}\frac{\partial [u]}{\partial z} + \frac{N^2}{f_0}W^* = \frac{\kappa Q^*}{f_0 H} \equiv R^*, \qquad (6.31)$$

where Q is the heating rate per unit mass and $\kappa = R/c_p$. As in Section 6.4, we assume a channel geometry, with $[u]$ and N^2 functions of z only, and with $[u] > 0$. The structure of the forced response depends crucially on whether the diabatic heating is balanced primarily by horizontal advection, either zonal or meridional, or primarily by adiabatic cooling. Which of these limiting balances holds, if either, is determined by the vertical structure of the heating as well as by the structure of the mean flow. The limit in which horizontal advection dominates is the more relevant for extratropical forcing, as argued below. Our discussion is based on that of Dickinson (1980) and Hoskins and Karoly (1981).

If horizontal advection balances the diabatic heating, one can obtain a particular solution by ignoring W^* in Eqn. (6.31) and solving for ψ^*. Noting that $[u]\,\partial\tilde{\psi}/\partial z - \tilde{\psi}\,\partial[u]/\partial z = [u]^2(\partial/\partial z)(\tilde{\psi}/[u])$, one finds for the Fourier amplitudes $\tilde{\psi}$:

$$\tilde{\psi}_p = \frac{i[u]}{k} \int_z^\infty \frac{\tilde{R}}{[u]^2}\,d\mu. \tag{6.32}$$

From the linearized vorticity equation:

$$ik[u](K_s^2 - K^2)\tilde{\psi}_p = \frac{f_0}{\rho_0}\frac{\partial}{\partial z}(\rho_0\tilde{W}_p) \tag{6.33}$$

where $K_s^2(z) \equiv \beta/[u]$, one then obtains for the vertical velocity:

$$\tilde{W}_p = \frac{-ik}{f_0\rho_0}\int_z^\infty \rho_0[u](K_s^2 - K^2)\tilde{\psi}_p\,d\mu. \tag{6.34}$$

The full linear response consists of this particular solution plus a homogeneous solution, denoted by a subscript h, chosen so that $W_h(0) + W_p(0) = 0$ (in the absence of topography and Ekman pumping). It is convenient to think of this homogeneous solution as forced by an 'equivalent topography':

$$\tilde{h}_T = -i\tilde{W}_h(0)/(k[u(0)]$$

$$= \frac{1}{f_0\rho_0(0)[u(0)]}\int_0^\infty \rho_0[u](K_s^2 - K^2)\tilde{\psi}_p\,d\mu. \tag{6.35}$$

The consistency of this solution can be checked by noting whether or not $N^2\tilde{W}_p/f_0$, with $\tilde{W}_p$ defined by Eqn. (6.34), is indeed negligible in Eqn. (6.31). This check is particularly simple if $[u]$ can be taken as uniform within the source region and Q can be assumed to have a simple vertical scale, $H_Q \propto |Q/(\partial Q/\partial z)|$ that is smaller than or comparable to the scale height of the atmosphere. For then:

$$\tilde{\psi}_p \propto RH_Q/(k[u]) \quad \text{and} \quad \tilde{W}_p \propto Rf_0^{-1}H_Q^2(K_s^2 - K^2),$$

and we have consistency if and only if:

$$\varepsilon \equiv N^2 f_0^{-2} H_Q^2 (K_s^2 - K^2) \ll 1. \tag{6.36}$$

In the extratropical lower troposphere, $K_s^2 \gg K^2$ for the planetary scale waves of interest. Making use of this approximation, one finds for the parameters in Fig. 6.14 that Eqn. (6.36) reduces approximately to $(H_Q/6 \text{ km})^2 \ll 1$.

If $[u]$ cannot be taken as constant with height this consistency condition will be altered. In particular, if the second rather than the first term in Eqn. (6.31) dominates, that is, if $H_u \propto |[u]/(\partial[u]/\partial z)| \ll H_Q$ within the region of diabatic heating, then $\tilde{\psi}_p \propto RH_u/(k[u])$, and H_u replaces H_Q in Eqn. (6.36). For the not untypical parameters in Fig. 6.14, $H_u \simeq 3$ km in the lower troposphere, so we still expect the consistency condition to be reasonably well satisfied for extratropical lower tropospheric heating.

The particular solution [Eqn. (6.32)] always possesses a low pressure centre a quarter wavelength downstream from the heating maximum. (We assume for simplicity that $\tilde{Q}$ has no phase variation with height.) Whether this is a cold or warm low depends on the vertical structure of the heating. If $H_Q \ll H_u$, so that zonal temperature advection is dominant in Eqn. (6.31), then the downstream low is warm. If meridional advection is dominant, $H_u \ll H_Q$, then the low is warm (cold) if Q decreases (increases) with height.

According to Eqn. (6.35), the equivalent topography is in phase with $\tilde{\psi}_p$ if $K < K_s$. Using Fig. 6.16 as a guide, one sees that for relatively short waves (but not so short that $K > K_s$ at low levels) the particular and homogeneous solutions are in phase, whereas for the longer waves that propagate into the stratosphere the homogeneous solution is shifted less than half a wavelength upstream. The scaling arguments of the preceding paragraphs suggest that within the source region,

$$|\psi_h/\psi_p| \propto \varepsilon/(m \min (H_Q, H_u)),$$

where m is the local vertical wavenumber of $\tilde{\psi}_h$. Even though ε may be considerably less than unity, m^{-1} is generally larger than H_Q or H_u, so ψ_h need not be entirely negligible within the heated region. If ψ_p does dominate, then one should see a gradual transition from ψ_p to ψ_h as z increases. For the long propagating waves, this implies a rapid westward phase shift with height that is distinct from the westward phase shift in the homogeneous solution itself.

Whatever the relative importance of ψ_p and ψ_h within the heated region, the magnitude of ψ_p will decrease away from the source and ψ_h will eventually dominate, having precisely the same characteristics as the orographically forced waves discussed in Sections 6.3 and 6.4. For a localized source, the far field will once again be dominated by equivalent barotropic external Rossby waves with the appropriate local stationary wavelength and with maximum amplitude near the tropopause.

In the opposite extreme, in which adiabatic cooling is primarily responsible.

for balancing the diabatic heating, a particular solution can be obtained by setting $\tilde{W}_p = f_0 N^{-2} \tilde{R}$ and substituting into the vorticity equation to obtain:

$$\tilde{\psi}_p = \frac{-i f_0^2}{[u] k \rho_0 (K_s^2 - K^2)} \frac{\partial}{\partial z}\left(\frac{\rho_0 \tilde{R}}{N^2}\right). \tag{6.37}$$

If the heating is non-zero at the ground, a homogeneous solution with $\tilde{W}_h(0) = -f_0 N^{-2} \tilde{R}(0)$ must be added, corresponding to flow over the equivalent topography

$$\tilde{h}_T = \frac{i f_0}{N^2 k [u]} \tilde{R}(0).$$

A similar argument to that leading to Eqn. (6.36) yields $\varepsilon \gg 1$ for the consistency condition. Typically, this condition will be met for deep sources in subtropical latitudes. Assuming once again that $K \ll K_s$, one finds from Eqn. (6.37) that low pressure is found a quarter wavelength downstream (upstream) from the heating maximum if $\rho_0 R N^{-2}$ decreases (increases) with height. A solution for a tropical heat source is shown in Fig. 9.22. The feature which is most apparent in the height field perturbation is the 'great circle' poleward propagation of the equivalent barotropic external Rossby waves.

6.6 The relative importance of thermal and orographic forcing

Whereas with linear models one often starts with the simplest dynamical framework and then adds complications one by one, in research with general circulation models one often takes the opposite approach, starting with a very detailed model with which one attempts to simulate the observed climate as best one can. One then uses this model as a surrogate atmosphere to be experimented upon, removing some physical process or simplifying some boundary condition to determine its importance for maintaining the climate. The comparison of a GCM with realistic orography and one with a flat lower boundary is an excellent example of this approach.

Several 'mountain'–'no-mountain' comparisons of this kind have been published, the most detailed being that of Manabe and Terpstra (1974). Rather than attempting to review these studies, a few preliminary results are presented from recent calculations performed at the Geophysical Fluid Dynamics Laboratory/NOAA, conducted with a relatively low-resolution spectral model (15 wave rhomboidal truncation). The distinctive feature of these calculations is the length of the integrations: the two experiments were each integrated for 15 model years after having reached statistically steady states. The reduction in sampling errors hopefully puts the dynamical interpretation of the difference between the two time-averaged flows on a surer footing. The long

integrations also allow one to analyse the model's low-frequency variability, as described by Manabe and Hahn (1982) and in Chapter 5. Both models have the identical sea-surface temperatures prescribed as a function of time of year and both have the same realistic continental distribution. The calculations were performed by S. Manabe and D. Hahn.

It has often been pointed out that the difference between the mountain and no-mountain climates cannot be interpreted as simply due to the mechanical diversion of flow by the mountains, since the insertion of the mountains has some effect on the distribution of the diabatic heating as well. Figure 6.19 shows the diabatic heating at 850 mb in both experiments, averaged over the 15 winter seasons. Although there is more small-scale structure in the heating when mountains are present, the large-scale patterns are quite similar. On the bases of such comparisons, we suspect that the interaction between the orographic and thermal sources may be of less importance than the nonlinear interaction between the forced wave fields themselves. With these provisos in mind, we shall persist in referring to the eddy field in the no-mountain model as the 'thermally forced' component and the difference between the mountain and no-mountain eddy fields as the 'orographically forced' component, the total eddy field being the sum of these two parts.

Figure 6.20 displays these two components, as well as the total field, for the geopotential at 45°N averaged over the 15 winter seasons. The total field can be compared with the observations in Fig. 2.3. The model provides a reasonably good approximation to the amplitudes of the major highs and lows in this section, the most noticeable discrepancy being the underestimation of the strength of the high centered at 20W and 250 mb at this latitude in the observations. The tendency for these geopotential fields to reach their maximum amplitudes near the tropopause is apparent both in the model and the observations, implying that much of this wave field can be thought of as vertically propagating in the troposphere but evanescent in the stratosphere (see Section 6.4). It is precisely the disturbances trapped within the troposphere that can be expected to be handled well by a GCM with most of its resolution within the troposphere (6 of 9 vertical levels in this case) and with an artificially reflecting upper boundary condition. Propagation into the stratosphere is more evident at higher latitudes, as is clear in the observed cross-section at 60°N.

One sees from the figure that the two components have rather different structures. The thermally forced eddies are of larger scale than the orographically forced eddies, particularly in the upper troposphere. They also have a larger and more systematic westward phase shift with height and show somewhat less of a tendency toward maximum amplitude at the tropopause—all plausible consequences of the larger zonal scale.

That the heating has larger scale than the orography might seem surprising, at least if one thinks of the very localized sensible heating of the atmosphere off
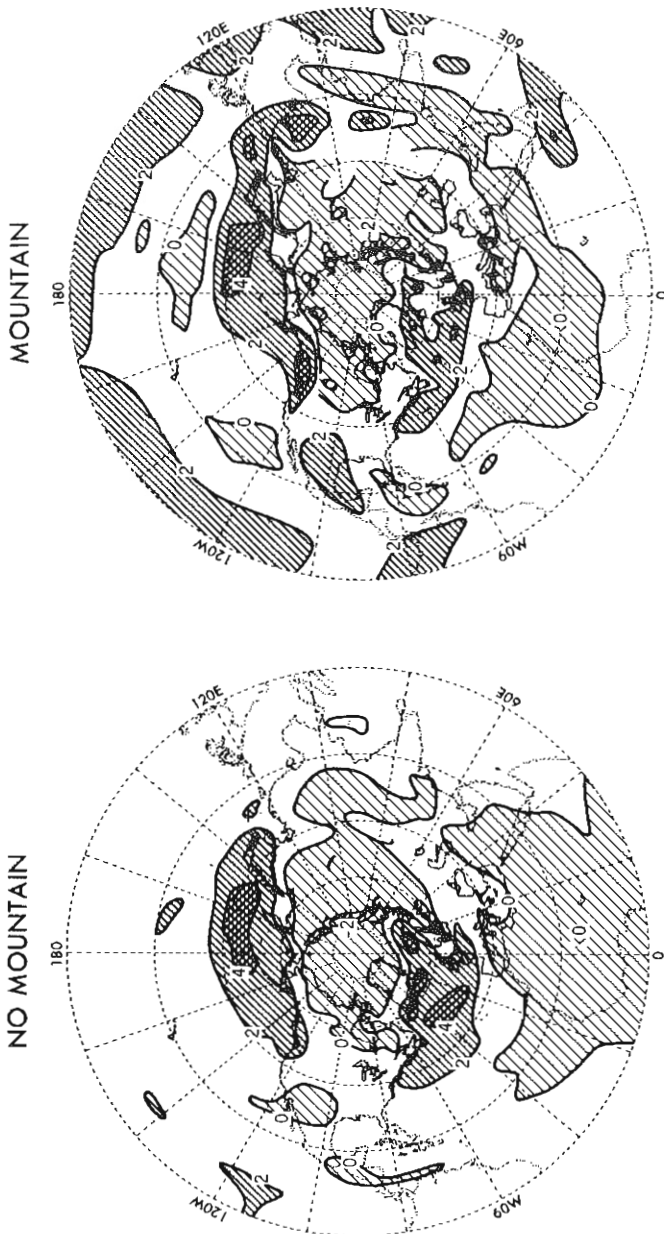
Fig. 6.19. The distribution of diabatic heating at 850 mb in the mountain and non-mountain models. The contour interval is 1 K day. Labels on contours should be multiplied by 0.5 K day.
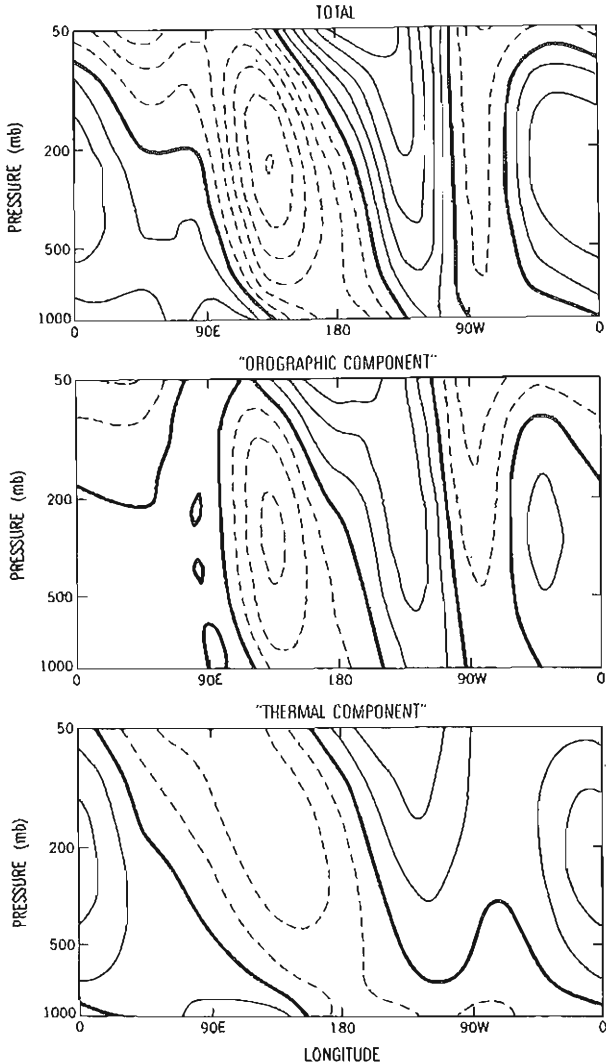
Fig. 6.20. The eddy geopotential height as a function of longitude and pressure at 45°N for the mountain model ('total'), the mountain minus no-mountain flow ('orographic component') and the no-mountain model ('thermal component'). The contour interval is 50 m with negative contours dashed. Model fields in Figs. 6.19–6.23 are averaged over the three winter months in each of the 15 model years.

the east coasts of the continents in the winter as being dominant. In fact, this sensible heating is dominant in the model only below 850 mb. At 850 mb (Fig. 6.19), the very large heating rates over the oceans at 45°, exceeding 2.5 K d^{-1}, are almost entirely due to latent heat release, whereas radiative cooling
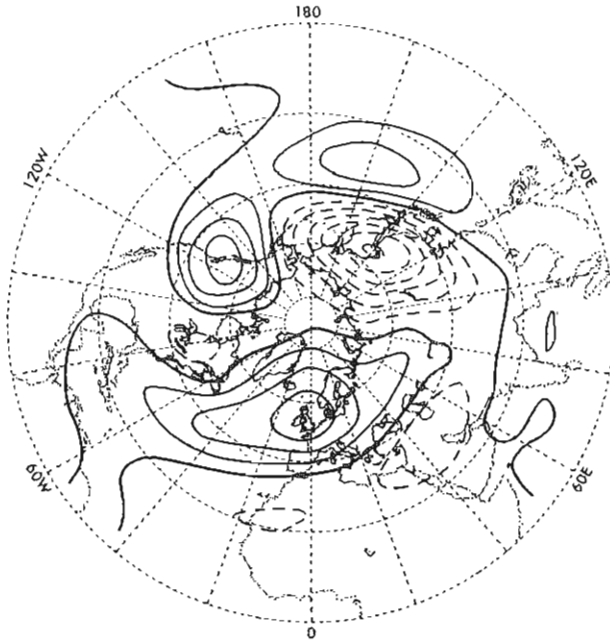
Fig. 6.21. The stationary eddy geopotential height at 300 mb in the mountain model. The contour interval is 50 m. Solid contours are positive or zero; dashed contours are negative.

dominates in the centres of the large continents. The latent heating maxima correspond roughly to the two major oceanic storm tracks. A theory for the thermally forced stationary eddies thus requires a theory for the location of the storm tracks.

Comparison with the topography used by the model (Fig. 6.5) shows that the scale of the topography is indeed somewhat smaller than that of the time-averaged heating. Even if the heating and orography had similar horizontal scales, the response to the orography would have the smaller scale, since it is $\partial h_T/\partial x$ rather than h_T itself that enters the boundary condition (cf. the k^{-1} factor in the 'equivalent topography' for thermal sources defined in Section 6.5). We have argued in Section 6.3 that the topography is sufficiently localized that the scale of the response is the scale of the stationary external Rossby wave rather than that of the topography itself. The scale of the time-averaged heating, on the other hand, seems to be sufficiently large compared with this stationary wavelength that the scale of the thermally forced component does reflect the scale of the heating. (Anomalies in the heating can have much smaller scales than the time-averaged heating, of course.)

The 300 mb geopotential height in the mountain experiment is shown in Fig. 6.21 and the separation into thermal and orographic components in Fig.

THERMAL COMPONENT   OROGRAPHIC COMPONENT
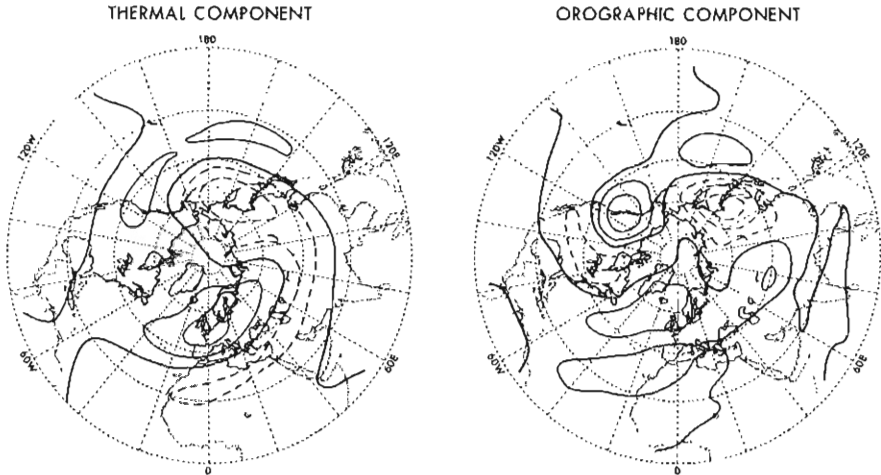
Fig. 6.22. The stationary eddy geopotential field of Fig. 6.21 split into its 'thermal' and 'orographic' components.

6.22. The two parts of the eddy field are of the same order of magnitude, but the smaller scale of the orographic component is again apparent. Because of this smaller scale, the orographic component should be more dominant in the meridional velocity and vorticity fields than in the geopotential. Constructive interference between the two components is evident in the Western Pacific and in the high at the Greenwich meridian and 50°N. There is destructive interference, if anything, over North America.

The streamfunction for the difference in the flows at 300 mb between the mountain and no-mountain models is shown in Fig. 6.23. The wavetrain structure is now more evident. There is a fairly close correspondence between the structure of the wavetrain between 120W and 60W and the linear waves forced by the Rockies in Fig. 6.9, and similarly for the high–low couplet in the Western Pacific and the linear response to the Tibetan plateau. The wavetrain oriented north–south near 0° longitude also seems to resemble a wavetrain at this longitude in the linear Tibetan response, although not in detail.

A comparison of the sea-level pressures in the two experiments in Fig. 6.24 shows that the Icelandic and Aleutian lows are present in full force in the no-mountain model. In fact, the Icelandic low is weakened substantially when mountains are inserted (while the Aleutian low is strengthened slightly). These experiments are consistent with the long-held belief that thermal effects are dominant near the surface, a belief based on the seasonal reversal of the surface pressure pattern. As is clear from Fig. 6.20, however, the topographic response is not negligible at the surface.

An interesting feature of the models' stationary waves is the correlation.
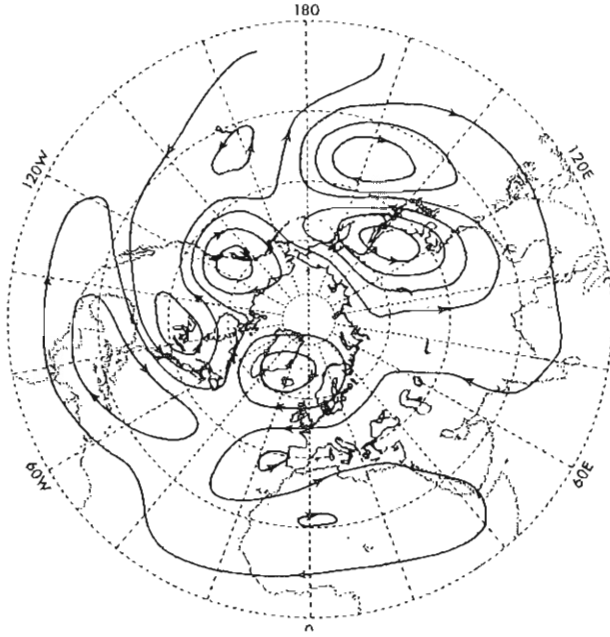
Fig. 6.23. The streamfunction for the mountain minus no-mountain flow at 300 mb. Contour interval is 4×10^6 m^2 s^{-1}.

between u^* and v^* near the maximum in the poleward momentum flux. The mountain and no-mountain models produce similar correlation coefficients of $\simeq 0.8$, as does the difference flow field. This is much higher than the observed value of $\simeq 0.4$ in Oort and Rasmussen (1971) discussed in Section 6.3. Primarily as a result of this difference, the model overestimates the standing eddy momentum flux by nearly a factor of three (the eddy velocities also being somewhat too large). This error in the stationary eddy flux is nearly compensated by an error of opposite sign in the transient eddy flux. Why compensation of this sort should occur is not clear.

Following the discussion in Section 6.3, we interpret this anomalously high correlation as resulting from the absence of Rossby waves of sufficient amplitude propagating polewards from the tropics into midlatitudes. Two alternative explanations exist for this deficiency: either tropical thermal sources of poleward propagating Rossby waves are not sufficiently active; or reflection of the equatorward propagating wavetrains is not occurring because of the absence of upper tropospheric easterlies (see Fig. 6.6). In any case, one can conclude from the absence of significant poleward propagation in the sub-tropics that the asymmetries in the extratropics of the no-mountain GCM are forced by thermal asymmetries in the extratropics rather than the tropics.

164
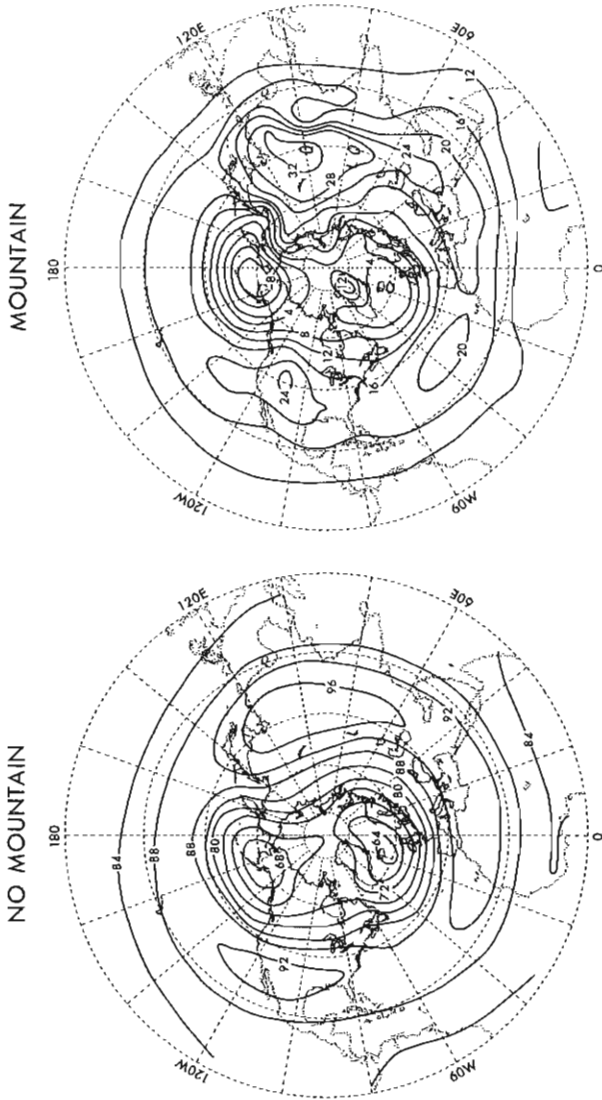
Fig. 6.24. The sea-level pressure for the mountain and no-mountain calculations. xx mb should be read 10xx mb for the mountain model and 9xx mb for the no-mountain model.

6.7 Quasi-stationary eddies in a zonally symmetric climate

It is tempting to assume that the quasi-stationary eddies in the atmosphere are closely related to the forced waves discussed in previous sections, the absence of strict stationarity being due either to variations in thermal sources and in the flow over the mountains, or to variations in the environmental flow through which the waves propagate. The teleconnection patterns described, for example, by Wallace and Gutzler (1981) and Horel and Wallace (1981) do resemble the Rossby wavetrains that, according to the arguments in Section 6.4, dominate the response to a localized source. The structure of the quasi-stationary eddies in a model that has no strictly stationary eddies, that is, in a model with a zonally symmetric lower boundary and zonally symmetric climate, clearly has some bearing on this hypothesis.

The model analysed is identical to the spectral GCM discussed in Section 6.6 and in Chapter 5, except that the realistic lower boundary condition is replaced by a flat land surface, and the seasonally varying solar flux is replaced by its annual mean values. The model statistics are thus stationary in time as well as homogeneous in longitude. In addition, surface albedos are fixed and the land is assumed to be always saturated, removing the potential sources of low-frequency variability in snow albedo-feedback and ground hydrology. Cloudiness is fixed in all of these models. The magnitude of the low-frequency variability in this idealized model, as measured by the standard deviation of monthly-mean geopotential height, is comparable to that in the model discussed in Chapter 5 that produces blocking episodes that are at least superficially realistic.

One aspect of the structure of the low-frequency variability in the idealized model is illustrated in Fig. 6.25, a plot of the correlation coefficient between the 300 mb monthly-mean meridional velocity at a reference point ($\simeq 45°$ latitude, $0°$ longitude) with the 300 mb monthly-mean meridional velocity at all other points on the sphere. (This field is computed using as a reference point each of the model's grid points along the latitude circle at $\simeq 45°$S; making use of the homogeneity of the statistics, these fields are all shifted to the same reference point and then averaged to produce the figure shown.) A similar plot using instantaneous rather than monthly-mean fields looks very different, the correlations dropping off more rapidly, with small negative correlations on either side of the peak at the reference point and only a hint of a wavelike structure.

This correlation field suggests that the low-frequency variability in the model is dominated by external Rossby wavetrains that happen to be nearly stationary because of their horizontal scale. The horizontal wavenumber in midlatitudes in Fig. 6.25 is 4–5, which is roughly what is needed for stationarity, the shape of the wavetrain resembles some of the ray paths
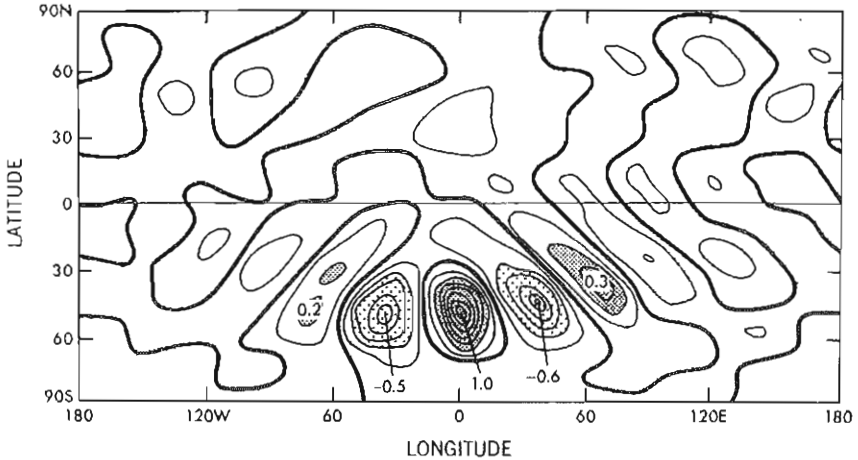
Fig. 6.25. The correlation coefficient between the monthly-mean 300 mb meridional velocity $v(\lambda, \phi)$ and $v(0, 45°S)$ for the model described in the text. The values of the local extrema of the correlation field are indicated.

computed by Hoskins and Karoly, and the phase tilts are just those expected for a wave propagating from west to east and reaching its turning latitude near the reference point. Examination of the vertical structure of the low-frequency variability shows these wavetrains to be equivalent barotropic with maximum amplitude near the tropopause, as expected for external Rossby waves.

It is rather surprising that the monthly-mean variability is dominated by such a well defined wavetrain, rather than some complex superposition of wavetrains passing through the reference point in different directions. One possible explanation is that it is that quasi-stationary wavetrain which has its turning latitude at the reference point that dominates the low-frequency variability at this point because meridionally propagating wavetrains generally attain their largest amplitudes near the turning latitude (see Hoskins and Karoly for a discussion of this point). In addition, Rossby waves are transverse; for a given streamfunction amplitude, meridional velocities are maximized if the wave is propagating east–west. Thus, one expects the variance of the meridional velocity to be dominated by that wave propagating east–west at the reference point, this being once again that wavetrain with a turning latitude at the reference point. The relevance of this last consideration is indicated by the fact that similar correlation maps computed using geopotential height or zonal velocity show a less wavelike pattern.

Discussion of the free external Rossby waves in the atmosphere is generally limited to the global normal modes which propagate westward sufficiently rapidly that they are not strongly affected by the structure of the mean winds, the wavenumber 1, 5-day wave being the best documented example (e.g.,

Madden, 1979). But Fig. 6.25 reminds us that a greater part of the energy in the external Rossby wave field is likely to be in somewhat smaller scales, in waves with small phase speeds with respect to the ground that are strongly refracted and perhaps absorbed by the mean flow. It is difficult, if not impossible, for these waves to organize themselves into global or hemispheric normal modes in the absence of significant reflection from low-latitude easterlies. They evidently exist primarily as wavetrains of the sort depicted in Fig. 6.25.

This analysis suggests an alternative to the point of view that low frequency circulation anomalies such as blocking highs are directly related to anomalous forced waves. Just as high-frequency cyclone waves would certainly exist in the absence of asymmetries in the lower boundary, but are organized into storm tracks by these asymmetries, so might the pre-existing external Rossby wave field be organized by these asymmetries to create preferred regions for low-frequency variability. How this might occur remains to be elucidated, although the large differences obtained by Simmons (1982) between small amplitude waves on zonally symmetric and asymmetric basic states is certainly suggestive.

Acknowledgements

References

BENNEY, D. J. and BERGERON, R. F. (1969). A new class of nonlinear waves in parallel flows. *Studies in appl. Math.*, 48, 181–204.

BOLIN, B. (1950). On the influence of the Earth's orography on the general character of the westerlies. *Tellus*, 2, 184–195.

CHARNEY, J. G. and DeVORE, J. G. (1979). Multiple flow equilibria in the atmosphere and blocking. *J. atmos. Sci.*, 36, 1205–1216.

CHARNEY, J. G. and ELIASSEN, A. (1949). A numerical method for predicting the perturbations of the middle latitude westerlies. *Tellus*, 1, 38–54.

CHARNEY, J. G., SHUKLA, J. and MO, K. C. (1981). Comparison of barotropic blocking theory with observation. *J. atmos. Sci.*, 38, 762–779.

DICKINSON, R. E. (1968). Planetary Rossby waves propagating vertically through weak westerly wind wave guides. *J. atmos. Sci.*, 25, 984–1002.

DICKINSON, R. E. (1980). *Orographic Effects on Planetary Flows*. GARP Publication Series, No. 23. W.M.O., Geneva.

GEISLER, J. E. and DICKINSON, R. E. (1974). Numerical study of an interacting Rossby wave and barotropic zonal flow near a critical level. *J. atmos. Sci.*, **31**, 946–955.

GEISLER, J. E. and DICKINSON, R. E. (1975). External Rossby modes on a β-plane with realistic vertical wind shear. *J. atmos. Sci.*, **32**, 2082–2093.

GROSE, W. L. and HOSKINS, B. J. (1979). On the influence of orography on large-scale atmospheric flow. *J. atmos. Sci.*, **36**, 223–234.

HAYASHI, Y. (1981). Vertical-zonal propagation of a stationary planetary wave packet. *J. atmos. Sci.*, **38**, 1197–1205.

HOREL, J. D. and WALLACE, J. M. (1981). Planetary-scale atmospheric phenomena associated with the southern oscillation. *Mon. Weath. Rev.*, **109**, 813–829.

HOSKINS, B. J. and KAROLY, D. J. (1981). The steady linear response of a spherical atmosphere to thermal and orographic forcing. *J. atmos. Sci.*, **38**, 1179–1196.

KAROLY, D. J. (1978). Unpublished lecture notes, NCAR Boulder, Colorado.

MADDEN, R. A. (1979). Observations of large-scale travelling Rossby waves. *Rev. Geophys. and Space Phys.*, **17**, 1935–1949.

MAK, M. (1978). On the observed momentum flux by standing eddies. *J. atmos. Sci.*, **35**, 340–346.

MANABE, S. and HAHN, D. G. (1981). Simulation of atmospheric variability. *Mon. Weath. Rev.*, **109**, 2260–2286.

MANABE, S. and TERPSTRA, T. B. (1974). The effects of mountains on the general circulation of the atmosphere as identified by numerical experiments. *J. atmos. Sci.*, **31**, 3–42.

NEWELL, R. E., KIDSON, J. W., VINCENT, D. G. and BOER, G. J. (1974). *The General Circulation of the Tropical Atmosphere and Interactions with Extra-tropical Latitudes*, Vol. 2. M.I.T. Press, Cambridge.

OORT, A. H. (1982). *Global Atmospheric Circulation Statistics, 1958–1973*. NOAA Professional Paper, U.S. Govt. Printing Office, Washington, D.C. (in press).

OORT, A. H. and RASMUSSON, E. M. (1971). *Atmospheric Circulation Statistics*. NOAA Professional Paper No. 5, U.S. Govt. Printing Office, Washington, D.C.

SIMMONS, A. J. (1982). The forcing of stationary wave motion by tropical diabatic heating. *Qt. Jl R. Met. Soc.*, **108**, 503–534.

SMAGORINSKY, J. (1953). The dynamical influence of large-scale heat sources and sinks on the quasi-stationary mean motions of the atmosphere. *Qt. Jl R. met. Soc.*, **79**, 342–366.

SMITH, R. B. (1979). In *Advances in Geophysics* (B. Saltzman, Ed.), Vol. 21, 87–230. Academic Press, New York and London.

TUNG, K. K. (1979). A theory of stationary long waves. Part III: Quasi-normal modes in a singular wave-guide. *Mon. Weath. Rev.*, **107**, 751–774.

TUNG, K. K. and LINDZEN, R. S. (1979). A theory of stationary long waves. Part II: Resonant Rossby waves in the presence of realistic vertical shears. *Mon. Weath. Rev.*, **107**, 735–750.

WALLACE, J. M. and GUTZLER, D. S. (1981). Teleconnections in the geopotential height field during the Northern Hemisphere winter. *Mon. Weath. Rev.*, **109**, 784–812.

WHITE, A. A. (1977). Modified quasi-geostrophic equations using geometric height as vertical coordinate. *Qt. Jl R. Met. Soc.*, **103**, 383–396.